A Portable Blood Coagulation Time Measurement Platform with Fiber-Optic Based Disposable Cartridge

by

Yusuf Samet Yaraş

A Thesis Submitted to the
Graduate School of Sciences and Engineering
in Partial Fulfillment of the Requirements for
the Degree of

Master of Science

in

Electrical and Electronics Engineering

Koç University

June 2016

Koç University

Graduate School of Sciences and Engineering

This is to certify that I have examined this copy of a master's thesis by

Yusuf Samet Yaraş

and have found that it is complete and satisfactory in all respects,
and that any and all revisions required by the final
examining committee have been made.

Committee Members:

_____

Prof. Dr. Hakan Ürey

_____

Asst. Prof. Dr. Fehmi Çivitci

_____

Asst. Prof. Dr. Sedat Nizamoğlu

Date: 29.06.2016

ABSTRACT

Advancements in sensor technologies have enabled miniaturized point-of-care (PoC) medical diagnostics devices and offer new opportunities in health care. Most of the new sensor platforms and lab on chip devices are still at laboratory level with only a few successful PoC implementations such as blood glucose monitoring devices. In this thesis, we focused on the development of a novel optical sensor platform and PoC device for periodic monitoring of blood coagulation, which is a critical need for cardiac patients on anticoagulant treatment.

While the golden standard for coagulation measurements is direct mechanical measurement from plasma in clinical laboratories, existing commercial and research phase PoC devices employ electro chemical and MEMS based lab on chip devices. This is the first report of a direct mechanical coagulation time measurement system designed for self-testing. The proposed platform has two parts; a disposable cartridge and a reader unit. Disposable cartridge has small volume microfluidic channels for blood flow and fiber optic based mechanical sensor. This sensor is composed of two optical fibers facing each other. One of the fibers is vibrated in mechanical resonance via an electro coil embedded in the reader unit. The other fiber is fixed and receives the light passing through the vibrating fiber. An optical AC signal is obtained at the output of the fixed fiber due to mechanically induced optical modulation. The reader unit has an LED light source coupled to the large core of the vibrating fiber, and a photodetector coupled to the the fixed fiber. Lack of electrical connection to the cartridge, remote electromagnetic actuation and optical read out enable simple and robust POC platform.

The proposed sensor platform is tested on a table top measurement set-up for activated-Partial-Thromboplastin-Time (aPTT) measurements on control plasma samples and human whole blood samples. Control plasma test results yielded <1% mean error and <1.36% relative standard deviation based on repeated tests. Then aPTT tests were successfully carried out with human whole blood samples. Proposed platform showed robust and repeatable results in both plasma and whole blood samples. A portable prototype based on table top measurement set up was developed in collaboration with SFO Technologies, India. aPTT test capability of the prototype was also demonstrated with human whole blood. Simplicity of the cartridge design and use of readily available materials enables low cost disposable cartridge and reader units. Future work will focus on reagent optimization, portable reader design, and validation of the system in clinical tests.

ÖZET

Sensör teknolojilerindeki gelişmeler küçültülmüş hasta başı testlerin (Point of Care diagnostics) gelişmesine olanak sağlayarak sağlık alanında yeni fırsatlar doğurdu. Hasta başı testlerinin birçoğu araştırma seviyesinde kalmış, pazardaki başarılı örnek sayısı birkaç uygulamayla, kan şeker ölçüm cihazı gibi, sınırlı kalmıştır. Bu uygulamalardan bir tanesi de kaz pıhtılaşma zamanı (koagülasyon) testidir. Herhangi bir kan inceltici tedavisi gören hastaların kan pıhtılaşma zamanlarının düzenli olarak ölçülmesi gerekmektedir. Bu tezin çalışmaları çerçevesinde fiber optik tabanlı kan pıhtılaşma zamanı ölçümü yapan bir sensör platformu geliştirildi.

Hasta başı kan pıhtılaşma zamanı ölçümü için elektro-kimyasal ve mikro kanal büzme gibi teknikler kullanılmasına rağmen klinik testlerde doğrudan mekanik ölçüm altın standart olarak kullanılmaktadır. Bu tezde sunulan çalışma, tam kan örneklerinden doğrudan mekanik ölçüm tekniği ile hasta başı kan pıhtılaşma zamanı ölçümü yapan ilk uygulamadır. Sunulan sensör platformu iki ana kısımdan oluşmaktadır: okuma ünitesi ve tek kullanımlık kartuş. Tek kullanımlık kartuşta kan akışını sağlaması için mikro akışkan kanalları ve ölçüm için fiber optik tabanlı mekanik sensör bulunmaktadır. Sensör, iki adet bir birine bakan optik fiberden oluşturmaktadır. Optik fiberlerden bir tanesi mekanik rezonans frekansında elektro mıknatıs sayesinde titreştirilerek diğer fibere eşleşen optik sinyal modüle ediliyor. Okuma ünitesinde bir adet optik fiber ile eşlenmiş ışık kaynağı ve bir adet optik fiber ile eşlenmiş foto detektör bulunmaktadır. Hem okuma hem de tahrik uzaktan yapıldığı için kartuşa herhangi bir elektrik bağlantı ihtiyacı yoktur.

Sunulan sensör platformu, tam kan ve kontrol plazma örnekleri kullanılarak aPTT ölçümleri laboratuvar düzeneğinde gerçekleştirildi. Kontrol plazması ile yapılan ölçümler %1'den küçük ortalama hata ve %1.36'dan küçük göreceli standart sapma ile sonuçlandı.

Tam kan testleri de benzeri sonuçlar verdi. Laboratuvar düzeneği baz alınarak SFO Technogies, Hindistan firması ile ortak çalışılarak bir adet hasta başı tanı cihazı prototipi geliştirildi. Geliştirilen prototiple de tam kandan aPTT test ölçümleri başarıyla yapıldı. Kartuş tasarımının basitliği ve hazır bulunan parçalardan üretilmesi düşük fiyatlı tek kullanımlık kartuş yapımını sağlamaktadır. Gelecek dönem çalışmaları, biyolojik ayraç optimizasyonu, taşınabilir okuyucu ünite tasarımı ve klinik testler üzerine yoğunlaşacaktır.

Bu tez çalışması çerçevesinde fiber optik tabanlı kan pıhtılaşma zamanı ölçümü yapan bir sensör platformu geliştirildi. Sensör platformu hem laboratuvar düzeneği hem de taşınabilir bir prototip şeklinde gerçeklenerek tam kan ve kontrol plazmaları ile aPTT testleri yapıldı.

ACKNOWLEDGEMENT

I am very grateful to my thesis advisor Prof. Hakan Ürey for providing his invaluable support and sharing his experience of research and life perspective. I would also like to thank Asst. Prof. Dr. Fehmi Çivitci for his endless help and kind friendship. I am also thankful to Asst. Prof. Dr. Sedat Nizamoğlu for taking part in my thesis committee. I am very grateful to Assoc. Prof. Dr. Göksenin Yaralıoğlu for his assistance through my thesis studies. I also want to thank Assoc. Prof. Dr. Ibrahim Barış for his help on coagulation biology.

It would have been impossible to complete my studies without the help of my colleagues and friends. I would like to thank Ali Bars Gündüz for his kind friendship and endless help, I finished my thesis on time thanks to him. I am also grateful that I had the chance to work with Gökhan Sağlam, he always watched my back. I am also thankful for other members of biosensor team: Deniz Ekin Canbay, Dr. Onur Çakmak, Fariba Ghaderinezhad, Aref Mostafazadeh, Celalettin Yurdakul, Özgün Civelekoğlu and Dr. Necmettin Kılınç. I always enjoyed working with them.

I am thankful to other members of OML for making it my home, to Ulaş Adiyan for his unique humour, to Sven Holmström for his endless conversations, to M. Kıvanç Hedili for fishing nights, to Uğur Aygün for cycling trip, to Deniz Mengü, Amir Ghanbariniaki, Dr. Erdem Ulusoy and Mahdi Kazempour for not disturbing me while sleeping on the couch. I also want to thank Shoaib Soomro for delicious Pakistani food. I also want to thank Kaan Akşit and Osman Eldeş for their help during my first months. I am also grateful to Gülüstan Eren for her help on paperwork and purchasing.

I would not be able to produce anything if it was not for Selim Abey. I am really grateful for his endless help and scolding. I really enjoyed warming friendship of Erhan Ermek. I am also grateful for the eternal friendship of Mehmet Serhan Can.

I would like to thank to Prof. Levent Değertekin from Georgia Institute of Technology for providing the opportunity to proceed research as a PhD student. I would like to thank Dr. Sarp Satır for his help and friendship.

I acknowledge TÜBİTAK 2211 Yurt İçi Lisansüstü Burs Programı for granting me a graduate student fellowship for my master's degree studies.

Finally, I would like thank to my family for their endless love and emotional support. Feeling their support was the main source of confidence and peace during the first steps in my academic career.

TABLE OF CONTENTS

LIST OF FIGURES

LIST OF TABLES

1 INTRODUCTION

In this chapter, Point of Care diagnostics are introduced. Blood coagulation physiology is briefly mentioned and state of the art blood coagulation sensors are reviewed for both clinical devices and point of care devices. Lastly, the contributions of this thesis are briefly presented.

1.1 Point of Care Diagnostics

Point-of-care testing is medical testing for diagnostic purposes near the patient's point of care, in the physician's office, at ambulance, at home, in the field, or in the hospital. It is usually used for either chronical diseases where periodic monitoring of specific values is vital or in critical conditions [1]. Point of care diagnostics' main goal is to provide accurate and timely test results for immediate and effective treatment [2]. Point of care tests must be simple to be conducted by either a medical technician or the patient himself depending on the application. Point of care devices' sizes can change depending on the application. They can be handheld, portable box sized or desktop sized. Handheld devices are produced generally for home usage whereas bigger sized ones are used in the field, ambulance or in the hospital. Point of care devices usually require small volumes of body fluids such as blood, urine or salvia[1]. A summary of Point of Care Testing (POCT) is given in Figure 1.1. In this thesis, point of care term is used specifically for handheld devices.

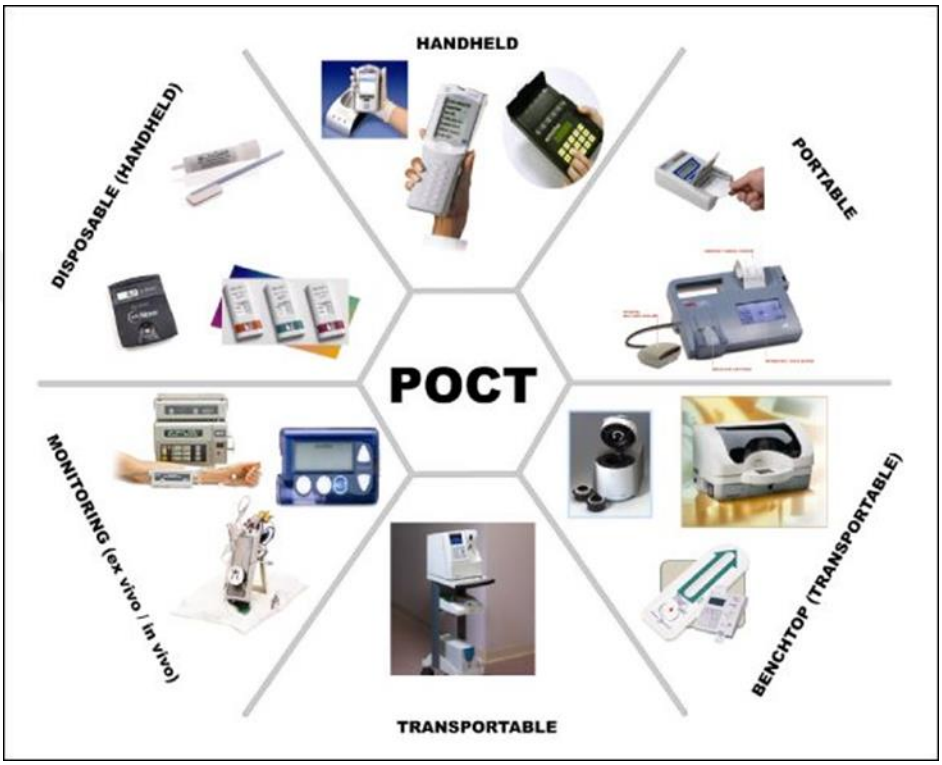

Figure 1.1 Different size Point of Care Testing (POCT) devices: handheld devices are intended for personal usage whereas less portable devices are intended to be used by technicians [3]

Glucometers are one of the most common PoC devices. Throughout the day, glucose level changes depending on diet or lifestyle[4]. Medication, regulates the glucose level in the blood of diabetes patients. Therefore medication dosage needs to be adjusted accordingly. Patients use glucometers, which measure glucose level in the blood, to determine their medication dosage or to contact with their physician for further help. Clinical laboratories cannot conduct tests as fast as portable glucometers and therefore physicians cannot respond in time.

Another point of care application is blood analyzers which are used for fast and easy assessment of patient state by providing information on blood content such as gases, lipids, enzymes etc[5]. Point of care blood analyzers can improve treatment results by providing short therapeutic turnaround time, especially for situations where time is a vital parameter for patient's survivability, such as in emergency rooms or in ambulances that immediate treatment is needed. Note that blood coagulation devices are not blood analyzers.

1.2 Blood Coagulation Measurement

Majority of cardiovascular patients use anticoagulant medicines and blood thinners. Their coagulation times should be measured periodically and the dosage of the anti-coagulant should be adjusted [6]. In this section, blood coagulation time measurements are discussed in detail.

1.2.1 Coagulation Physiology and Tests

Coagulation is process in which the blood changes its state from liquid to gel like consistency. When the blood vessels get damaged, hemostasis start in order to stop bleeding, and coagulation is the third step of this process. [7]. Coagulation is a complex process and there are several steps to it known as coagulation cascade. Figure 1.2 shows the pathways for coagulation process.

Coagulation starts immediately when endothelium layer of the blood vessel is damaged. Platelets circulating freely in the blood contact with collagens underneath the endothelium layer form a plug, known as primary hemostasis. Platelet plug itself is not sturdy enough for complete cease of bleeding, thus a secondary hemostasis starts

immediately [8]. When tissue factor beneath endothelium layer is exposed to blood, it reacts with plasma Factor VII and initiates a complex reaction series resulting in fibrin formation. Fibrin strands further strengthen the platelet plug thus complete hemostasis is achieved. Coagulation cascade of secondary hemostasis can be divided in three major groups: intrinsic pathway, extrinsic pathway and common pathway. Intrinsic pathway starts with primary collagen forming (surface contact) whereas extrinsic pathway starts with tissue factor (TF) exposure due to tissue damage. Common pathway is the last part of the coagulation cascade; fibrin clot is formed through several steps from prothrombin.

Blood coagulation testing measures clot formation time. Blood coagulation tests are required for patient assessment of different disease conditions or for treatment evaluation. Coagulation tests are required for patient condition evaluation before any operation [9], hepatic and renal disorders [10] or dengue hemorrhagic fever [11]. Patients receiving any anticoagulant treatment [12] and patients with or risk of cardiac problems such as embolism, atrial fibrillation or stroke need to undergo blood coagulation tests periodically [13] . Dosage of anticoagulants must be adjusted according to blood coagulation test results. Over 800 million coagulation tests are performed each year [14]. Therefore, reliable and fast coagulation assays are in demand [6], [15]. There are two type of coagulation tests practiced: Prothrombin time (PT) and activated partial thromboplastin time (aPTT) [16]. PT measurements are correlated to blood coagulation activation by tissue factor whereas aPTT measurements are correlated to activation by surface contact [17] . PT tests are conducted by adding a tissue factor reagent such as rabbit brain thromboplastin to plasma sample in order to initiate extrinsic pathway of coagulation cascade [18]. For aPTT tests, a mixture of phospholipids and activator such as silica, kaolin etc. is added to plasma sample to activate intrinsic pathway of coagulation cascade [19].

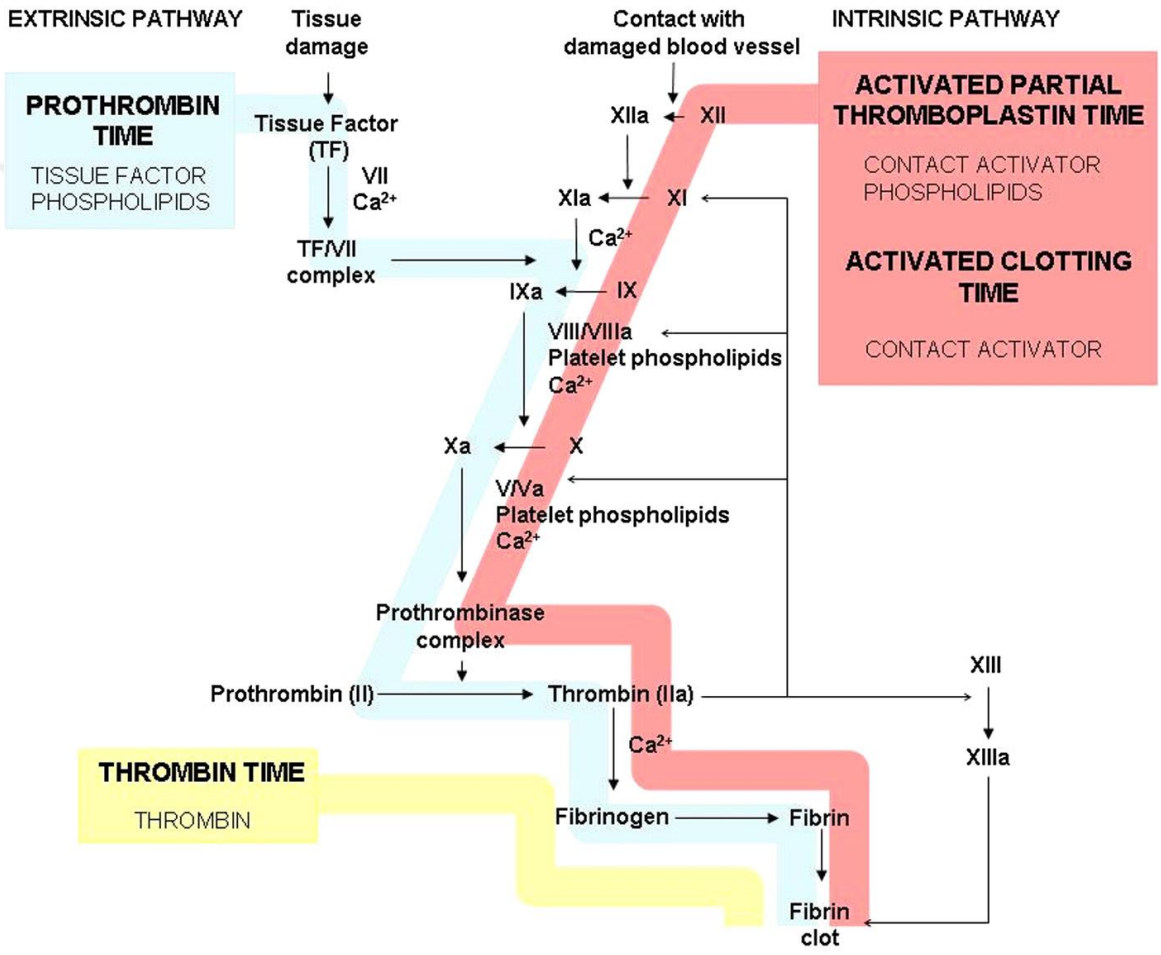

Figure 1.2 The coagulation cascade and clotting time tests. The coagulation cascade has two primary, interconnected pathways – extrinsic and intrinsic. Intrinsic pathway starts with primary collagen forming (surface contact) whereas extrinsic pathway starts with tissue factor (TF) exposure due to tissue damage. [6]

1.2.2 State of the art blood coagulation sensors

Blood coagulation measurements are conducted either in clinical laboratories or with POC devices. In the laboratory measurements, patients need to be in the hospital for sample delivery and a laboratory technician performs the coagulation tests. Thus, clinic coagulation tests set back both the clinics and patients in terms of time and money. Moreover, return time of coagulation time is vital in emergency situations such as in ambulances or during operations. Therefore, POC coagulation test devices are more convenient for patients whose coagulation time measurements need to be performed regularly and in emergency situations where return time is crucial. On the other hand, POC devices are usually not as accurate as clinic instruments [15]. Clinic tests are more convenient for diagnostic purposes where accurate test results are needed.

1.2.2.1 Clinical Devices

Clinic coagulation measurements are performed with plasma samples. Blood is drawn into anticoagulant tubes containing sodium citrate. Sodium citrate binds the calcium in the blood to prevent coagulation. Plasma samples are extracted from the calcium free blood by centrifuging. There are several coagulation detection techniques employed in clinical instruments. Those techniques can be divided into two major group: optic and mechanic [6]. Figure 1.3 gives an overview of clinical coagulation measurement techniques.

Coagulation monitoring devices based on optical detection uses turbidimetric [20] and nephelometric [21] techniques. Both turbidimetric and nephelometric techniques exploit optical density change in the plasma by fibrin formation. Transmittance and scattering of the plasma changes as fibrin strands are generated. Turbidimetric techniques monitors the

transmittance change of the plasma whereas nephelometric monitors change in scattering characteristics. BCS XP and Sysmex (Siemens Healthcare Diagnostics, USA) and ACL (Instrumentation Laboratories, USA) are examples of optical detection based coagulation monitoring devices used in clinical laboratories.

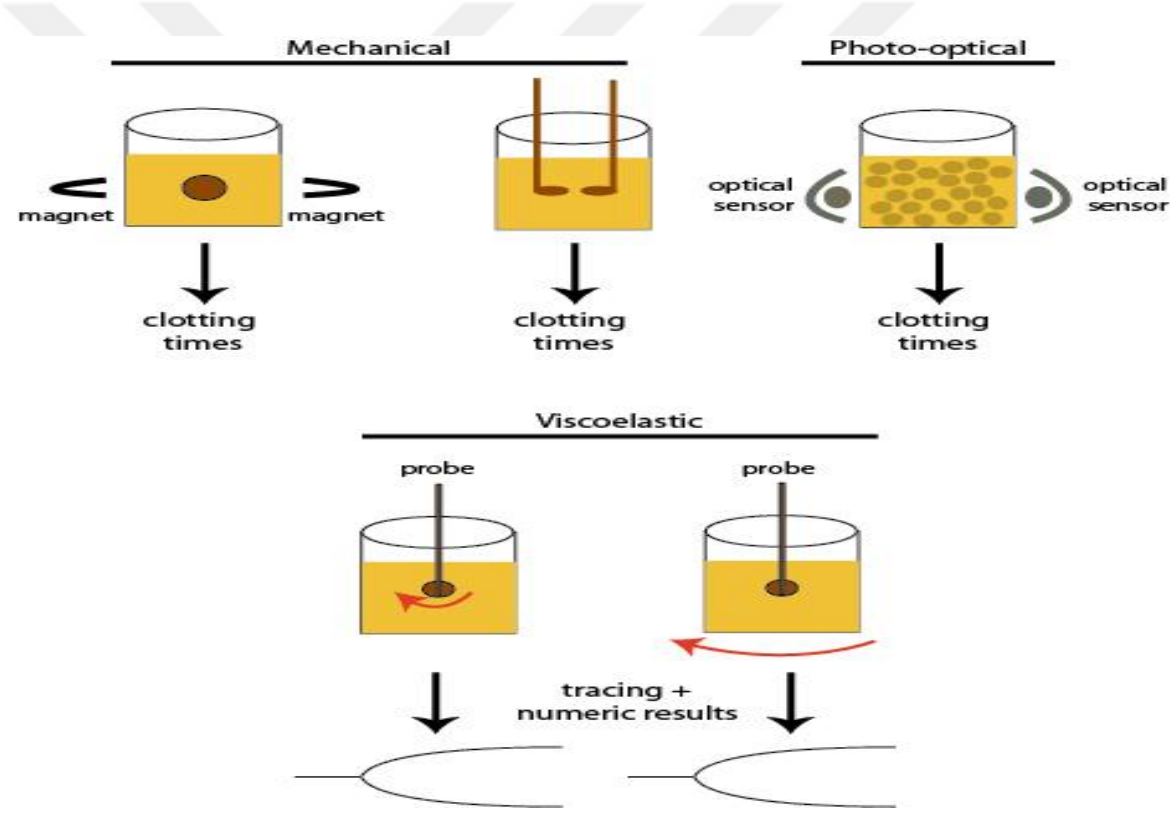

Figure 1.3 Coagulation monitoring techniques used in clinical devices. In mechanical detection method, detection method exploits viscoelastic characteristic change induced by clotting. Optical detection techniques rely on optical density change related to fibrin formation. All clinical coagulation measurements use plasma samples.

Direct mechanic coagulation measurement systems monitor viscosity change induced by clot formation. For example, a steel ball is moved inside the plasma sample by electromagnetic actuation [22]. Steel ball slows down and eventually stops due to increase in the viscosity of the plasma. Movement of the steel ball can be captured through an optical sensor. Another technique is rotating the plasma sample with a steel ball inside. Steel ball does not rotate with the sample thanks to a stationary permanent magnet closely placed to plasma sample[6]. Steel ball is trapped by the fibrin strands when coagulation occurs, thus steel ball starts to move with the plasma [23]. STA-R series (Diagnostica Stago, France) and KC series (Tcoag, Ireland) coagulation monitoring devices use mechanical measurement techniques. Figure 1.4 shows a fully automated high throughput hemostasis analyzer.

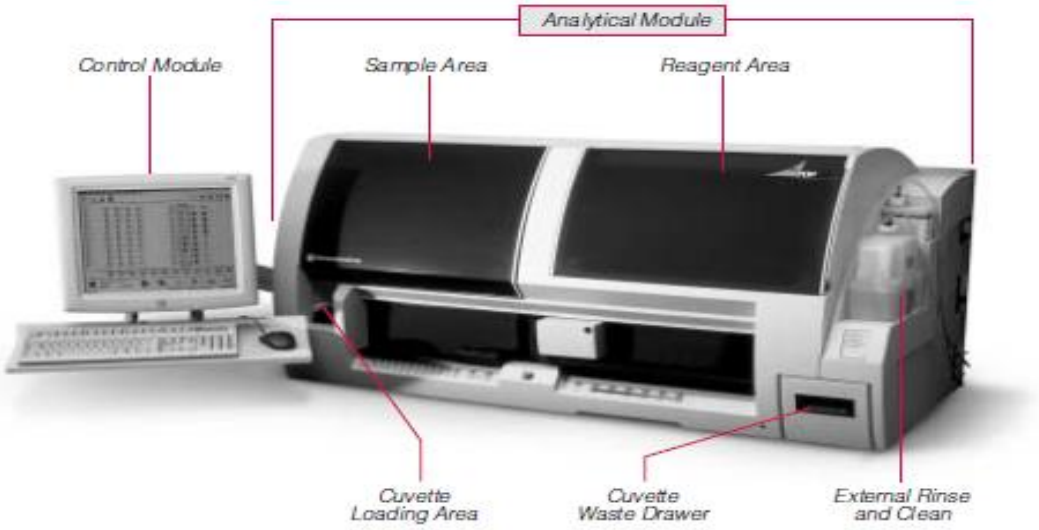

Figure 1.4 An example of fully automated high throughput hemostasis analyzer

1.2.2.2 Point of Care Devices

Point of Care coagulation monitoring devices need to be operated with whole blood samples [6]. Blood sample can be extracted from the patient by a finger stick or venipuncture. Blood samples are loaded to disposable cartridges or strips. For convenient use, measurements should be conducted using small volumes. Finger prick based blood collection methods usually result in 10-20 μL of useful blood volume [24]. Moreover, patients using glucometers are familiar with prick based blood collection.

There are two types of measurement principles extensively employed in PoC coagulation monitoring devices: micro fluidic constriction and electro-chemical detection with optical or resistive read out schemes.

Electro-chemical detection method exploits the electrical resistance change in the blood by coagulation. Electro-chemical based devices use two electrodes: working and reference. A constant potential voltage is applied to working electrode. An oxidation reduction reaction occurs resulting in an electrical current [25]. As blood coagulates, electro-chemical characteristics of the blood changes thus the induced electrical current. Electro-chemical based devices can operate with very small sample volumes with fairly easy cartridge or strips. Disadvantage of such devices are; indirect measurement of coagulation and chemical/ biological coating needs to be consistent for all cartridges since induced electrical current strongly depends on ionic composition of the blood [6] and compatibility issues with certain health conditions / dieses [26] may occur. The CoaguChek XS (Roche Diagnostics) and the i-STAT (Abbott Diagnostics) devices are examples for electro-chemical detection.

a)

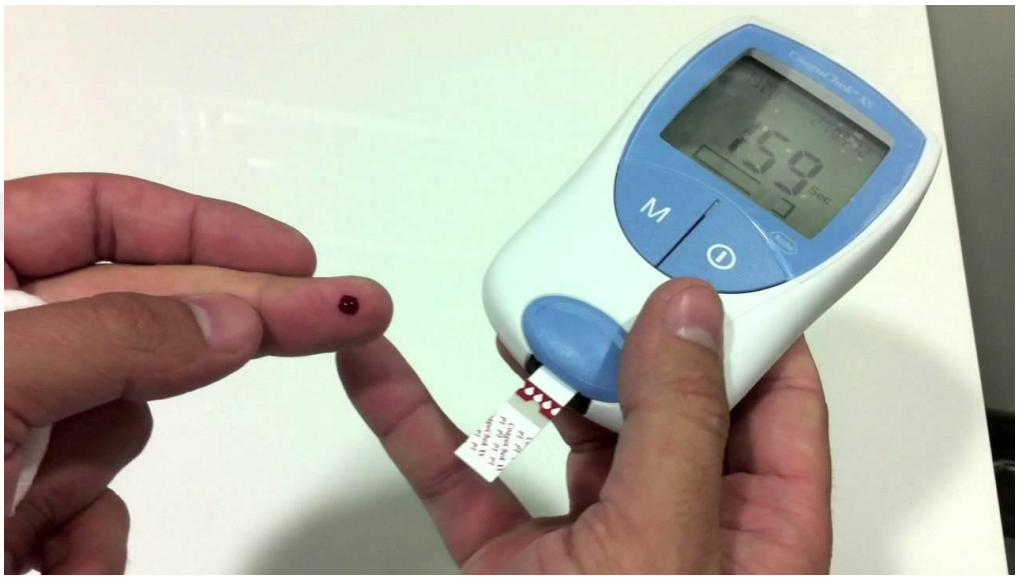

b)

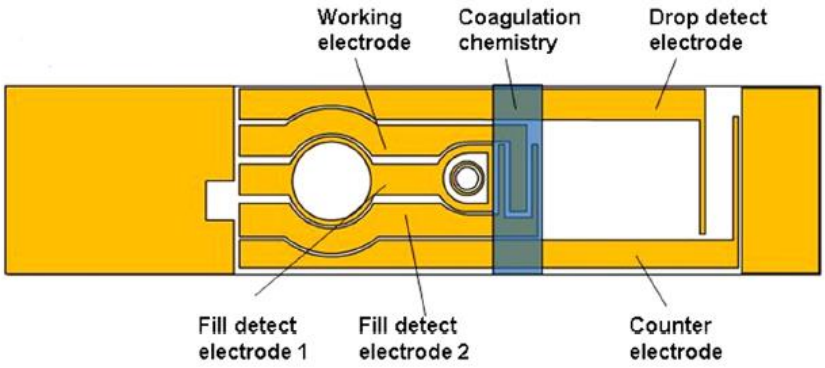

Figure 1.5 a) CoaguChek XS (Roche Diagnostics) in use with blood extracted using a finger prick b) CoaguChek XS (Roche Diagnostics) strip with electrodes for coagulation detection and timing/filling of the disposable sensor strip [6]

Micro fluidic constriction based detection methods utilize the flow rate change of the blood in a micro fluidic channel by clot formation. Read out is usually carried out with simple optical sensors. Blood sample can be either pumped through the micro fluidic channel (Hemochron Signature +, Signature Elite ITC, USA) or self-promoted by capillary motion (microINR, iLine Microsystems, Spain). Micro fluidic constriction based detection method is the closest technique available in the handheld PoC coagulation monitoring market to direct mechanical measurement technique which is golden standard in clinic instruments. However, micro fluidic cessation based devices are prone to hematocrit differences among individual users due to viscosity variation [27].

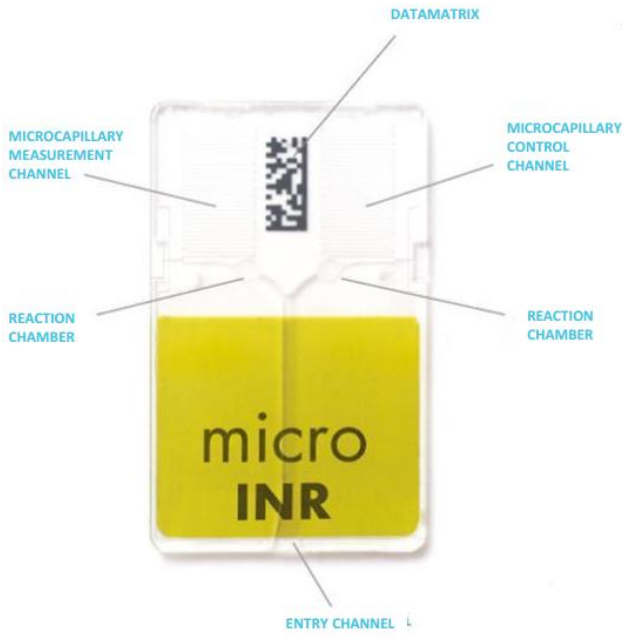

Figure 1.6 microINR cartridge showing two serpentine like micro fluidic channels with control and measurement sides

1.2.2.3 Novel Research Technologies in Coagulation Testing

Blood coagulation measurement technology is still a hot topic in research. There are several different methodologies and techniques applied in the literature. In this section, a selected number of new coagulation assessment technologies in research stage will be discussed.

Quartz crystal microbalance (QCM) is used in one of the studies for clotting detection [28][29]. QCM is a piezo-electrically actuated shear mode oscillator that is extremely sensitive to changes in physical properties at the surface. QCM resonators usually operate in high frequencies (10 MHz range) and have a penetration depth of 100-300 nm at the surface [6]. When fibrins are formed, viscoelastic properties of the samples at the surface change which alters resonance characteristic of the QCM. Work of Hussain showed 6.5% and lower RSD% in plasma samples with respect to a commercial device [29].

Optical based coagulation detection methods are also employed in literature. One study utilizes speckle pattern change induced by the clotting [30]. Another group employs optical coherence tomography with an acoustic transducer for both time measurements and quantitative mechanical characterization of fibrin strands giving further information to physicians about patients condition [31]. Figure 1.7 shows the measurement set-up with optical coherence tomography. Turbidimetric based detection methods are also applied to coagulation monitoring from whole blood samples [32][33].

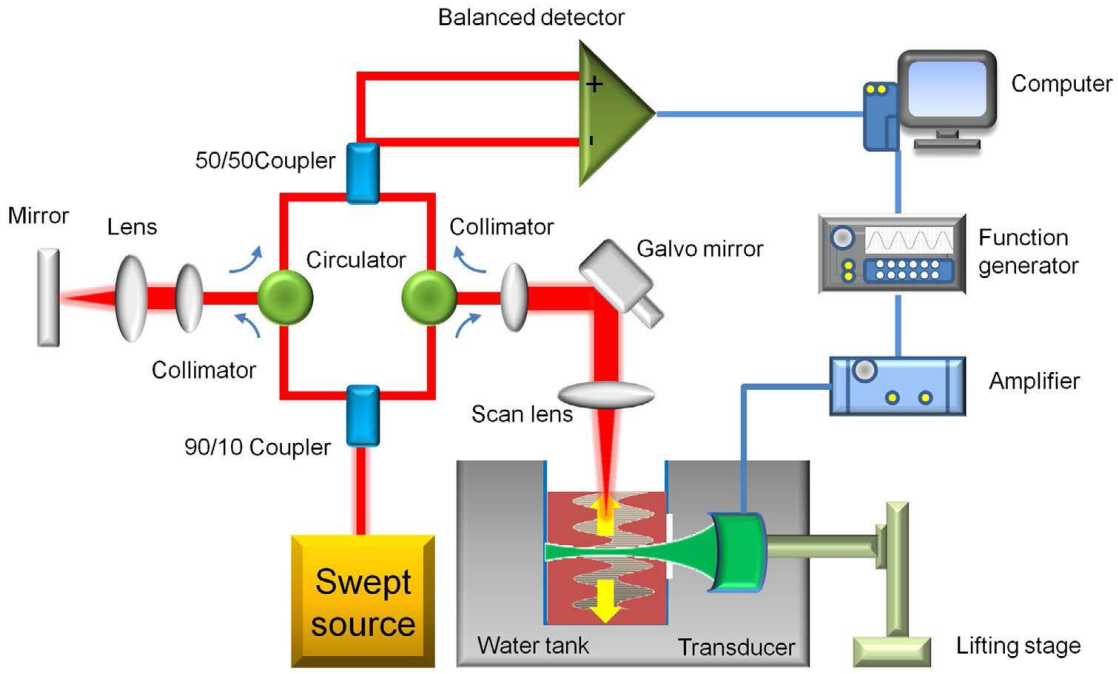

Figure 1.7 The schematic of the ARFOE-OCE system, including the swept source OCT unit and ultrasonic excitation unit. The vibration perpendicular to the OCT detection direction is detected by a Doppler variance method, and the shear wave propagating parallel to the OCT detection direction is measured by M-scans. The blood is filled to a box with a window of plastic wrap for the ultrasound wave passing. The box and the transducer are immersed in water for impedance matching of the ultrasound wave into the blood sample. Only the container contacts with the blood sample.[31]

Micro electro mechanical systems (MEMS) have become a popular technology for PoC devices due to compact sizes and cost effective solutions they offer as biosensors [34]. A MEMS based coagulation measurement platform has been developed for viscosity and plasma coagulation measurements by our group [35]–[38]. Figure 1.8 shows basic

measurement set-up for the system. MEMS cantilevers are vibrated in the plasma sample. Fibrin formation introduces hydrodynamic loading on the MEMS cantilevers and changes the resonant response of the cantilevers. Resonant behavior change can be tracked either by frequency tracking or amplitude and phase monitoring at fixed frequency. Different optical read out schemes were implemented such as diffraction based, Laser Doppler Vibrometer (LDV) based or fiber based.

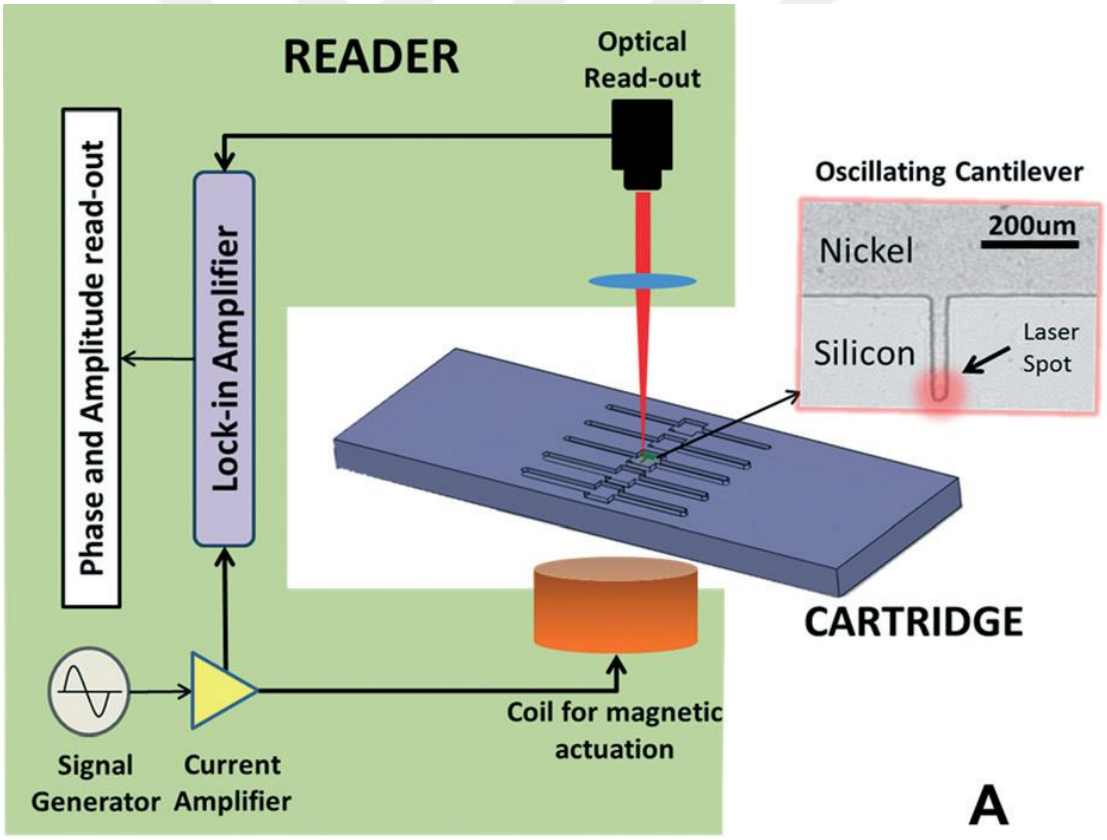

Figure 1.8 Schematic of MEMS based viscosity and plasma coagulation measurement system previously developed in our laboratory [35]

MEMS based system developed by our group yielded reproducible results with 7% or lower CV with respect the CoaguChek XS (Roche Diagnostics) using plasma samples. Due to complex nature of the whole blood, optical read out yielded low signal to noise ratio (SNR) optical signals. This issue could be solved by employing piezoelectric read out but it will increase the coast of individual sensors considerably. Another problem is assembly of the cartridges due to tight alignment tolerances, < 20 μm. Thus a new method was developed similar to MEMS based system as a more suitable platform for PoC coagulation monitoring market.

1.3 Contributions of the Thesis

This thesis reports a novel optical fiber based sensor platform for coagulation time measurements from whole blood. This work reports a direct mechanical coagulation time measurement system, which is gold standard in clinical devices, from whole blood samples designed for hand held point of care applications. Indeed we expect that success rate of the method will be higher than other PoC blood coagulation measurement systems available.

Previous work in our laboratory used MEMS cantilever sensors [35]–[37]. MEMS approach was found to be challenging due to (i) precision alignment difficulties between the external laser, MEMS cantilever array chip, cartridge, and the readout optics, and (ii) scattering of laser light by the red blood cells, which fills the gap between the top cartridge surface and the MEMS chip.

A novel optical sensor is developed during this thesis research to overcome the precision alignment and light scattering challenges. The novel optical sensor consists of two optical fibers with a small gap in between their tips mounted inside the disposable cartridge. In-coupling and out-coupling to the large core fibers in the cartridge proved relatively simple and has large mechanical tolerances. One of the fibers acts as one-end fixed cantilever with a moving tip vibrated remotely by an electro-coil whereas the other fiber is fixed. Thus an AC optical signal is mechanically induced to light coupled to the fixed fiber. Vibrated fiber cantilever is partially submersed in blood. Any change in the mechanical properties of the blood is monitored through optical signal. One of the contributions of this work is use of a fluid stop region in order to prevent fluid leakage in between fibers. Fluid stop region utilizes capillary action; therefore there is no physical barrier. High SNR optical read is obtained even in complex fluids such as whole blood thanks to the fluid stop region.

Design and fabrication aspects of the proposed novel optical sensor and the coagulation measurement system are discussed in detail in chapter 2. In chapter 3, proposed system was tested with activated-Partial-Thromboplastin-Time (aPTT) measurements. System was first characterized in different mediums; air, water, uncoagulated and coagulated plasma. The aPTT tests were conducted with control plasmas. Control plasma tests yielded <1% mean error and <1.36% relative standard deviation. Subsequently, whole blood aPTT capability was demonstrated using the sensor platform. Each test was repeated 3 times in order to demonstrate reproducibility of the measurements using proposed system. Thesis ends with conclusions and future work in chapter 4.

During this thesis research, a portable prototype was developed in collaboration with SFO Technologies, India. The reader unit optics, mechanics, and electronics were subsequently modified in our laboratory and became fully operational. Another design revision is required to make it ready for clinical trials and for point of care applications. A patent application has been filed for the proposed system and two journal articles have been drafted.

2 SYSTEM DESIGN AND FABRICATION

In this chapter, sensing platform is introduced with theoretical background and fabrication of the cartridges. The sensor platform is introduced and an overview of the working principles is given in section 2.1. Optical read out is discussed in Section 2.2 and theory of vibrating cantilever like structure discussed in Section 2.3. Opto-mechanical design aspect of system is given in Section 2.4. Cartridge design is discussed in Section 2.5 followed by brief explanation of cartridge fabrication in Section 2.6. Then individual components are introduced and specification for each component is given out in Section 2.7.

2.1 Working Principles of the Platform

In this section, working principles of the sensor platform will be explained briefly. Further detailed discussions about working principles will be given in the rest of Chapter 2. This section just serves as an introduction to the sensor platform and get the reader familiarize with it.

Schematic of the measurement set-up is shown in figure 2.1. Sensor platform consists of two units: a disposable cartridge and reader unit. Cartridge has two optical fibers and micro fluidic channels. One of the optical fiber is suspended in the microfluidic channel whereas the other optical fiber is secured in the cartridge wall. Fluid stop region is dramatically larger than rest of the micro fluidics creating a fluid stop region where two

end faces of the opposing fiber parts meet. Fluid stop region provides stable and low noise optical read out by preventing leakage of blood into the light pathway.

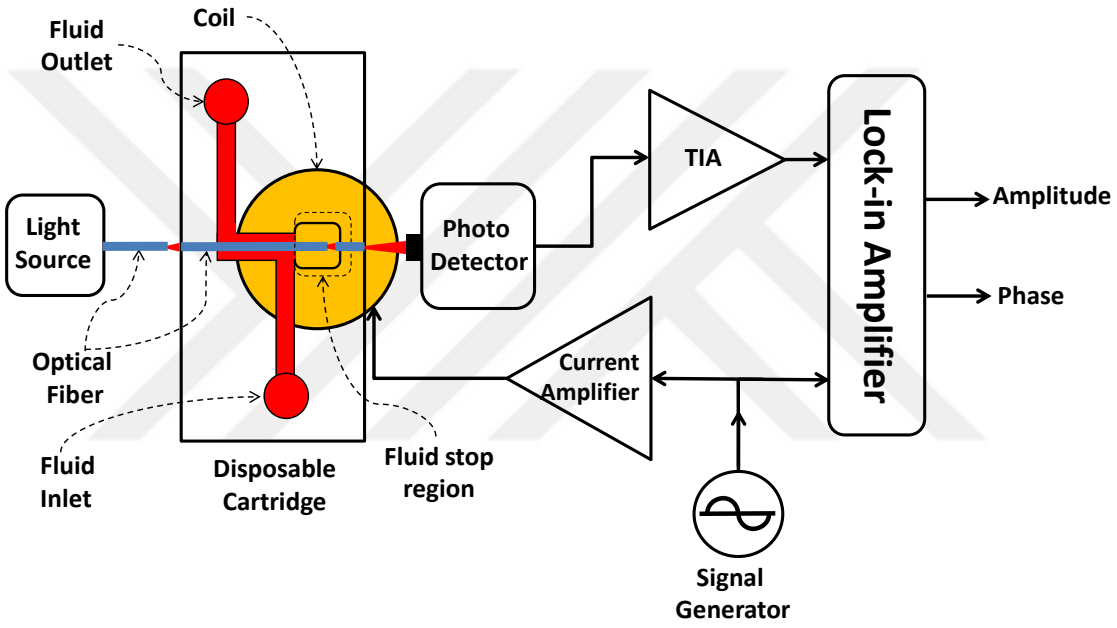

Figure 2.1 Schematic of the measurement set-up. Optical fiber is actuated is actuated remotely by an electro coil. Optical signal is collected through a silicon photo detector. Amplitude and phase is monitored by lock-in amplifier.

A nickel part is attached to the tip of suspended fiber. Fiber with nickel part is suspended in the sensor chamber and fluid stop region. Stationary fiber part acts as a receiver. Since fiber with nickel part is actuated, light coupled from moving fiber to receiving fiber is modulated. This modulated light is collected by the photo detector. When blood or plasma coagulates, a sudden change in viscosity occurs by clot formation.

Viscosity of the liquid in which a large portion of the vibrating optical fiber is immersed affects the resonance frequency and quality factor of the system.

Briefly, there are two force components of hydrodynamic loading; inertial and viscous. Inertial force is related to liquid mass that is moved by the vibrating structure whereas viscous force is related to the viscous drag of liquid medium resisting to movement of the vibrating structure. As viscosity of the liquid medium changes, resonance characteristic of the system also changes. Detailed explanation about hydrodynamic loading on cantilever like structures vibrating in viscous mediums can be found in Sader's study [39]–[41] When blood coagulates, viscosity of the system increases. Increase in the fluid medium causes decrease in resonance frequency and quality factor of the system. Change in resonance characteristic of the system can be tracked either by driving the system at constant frequency and monitoring phase and amplitude change or tracking the resonance frequency [42], [43]

2.2 Optical Sensor Design

Optical fibers have been utilized as cantilevers for mechanical sensing mechanism in the literature. Optical fiber cantilevers were utilized as accelerometers [44], [45]. In a recent study, optical fiber based sensor was used as an angular displacement sensor [46]. Another study has utilized a resonantly moving fiber as a viscosity sensor with optical read out from a polarized laser beam scattered by the moving fiber (note that laser beam for optical read out is not guided through the fiber) [47], [48].

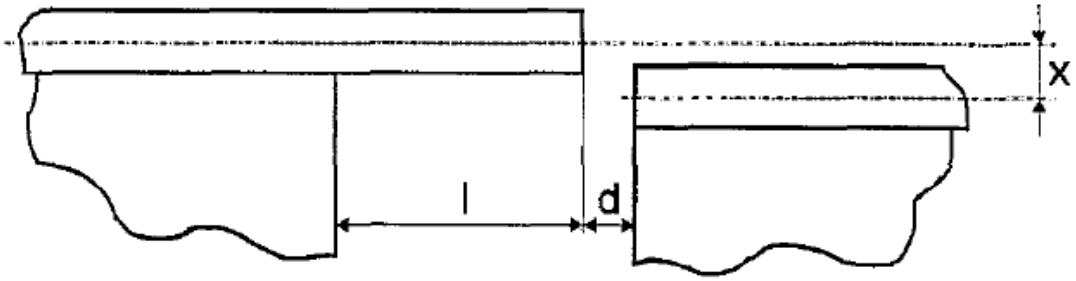

Figure 2.2 Sensor design with construction parameters: cantilever beam length (*l*), fiber- offset (*x*), air-gap width (*d*). [44]

Figure 2.2 shows the fiber based sensor structure used in this study. It is composed of two fibers, one which is suspended in the sensor chamber facing a stationary fiber. When suspended fiber is actuated, light coupled from moving fiber to receiving fiber is modulated. This modulated light is collected by the photo detector. Optical modulation induced by mechanical movement is determined by fiber geometry and offset between moving fiber and stationary fiber. Optical fibers were selected as a 400 μm core and 440 μm cladding diameter for better alignment tolerances during insertion of the cartridge into reader unit. Different offset values were simulated using ZEMAX software. Simulation results were confirmed with experimental data. Distance between two fibers *d*, was taken 250 μm for easy fabrication and fiber length *l* was taken 4 mm. Figure 2.3.a shows comparison between simulation and experimental data of transmittance for different offset values. As expected, coupled power decreases as offset increases. Optical modulation is given by the rate of change in coupled power with respect to offset distance as shown in figure 2.3.b. For maximum sensitivity, offset gap was chosen 120 μm with the given configuration.

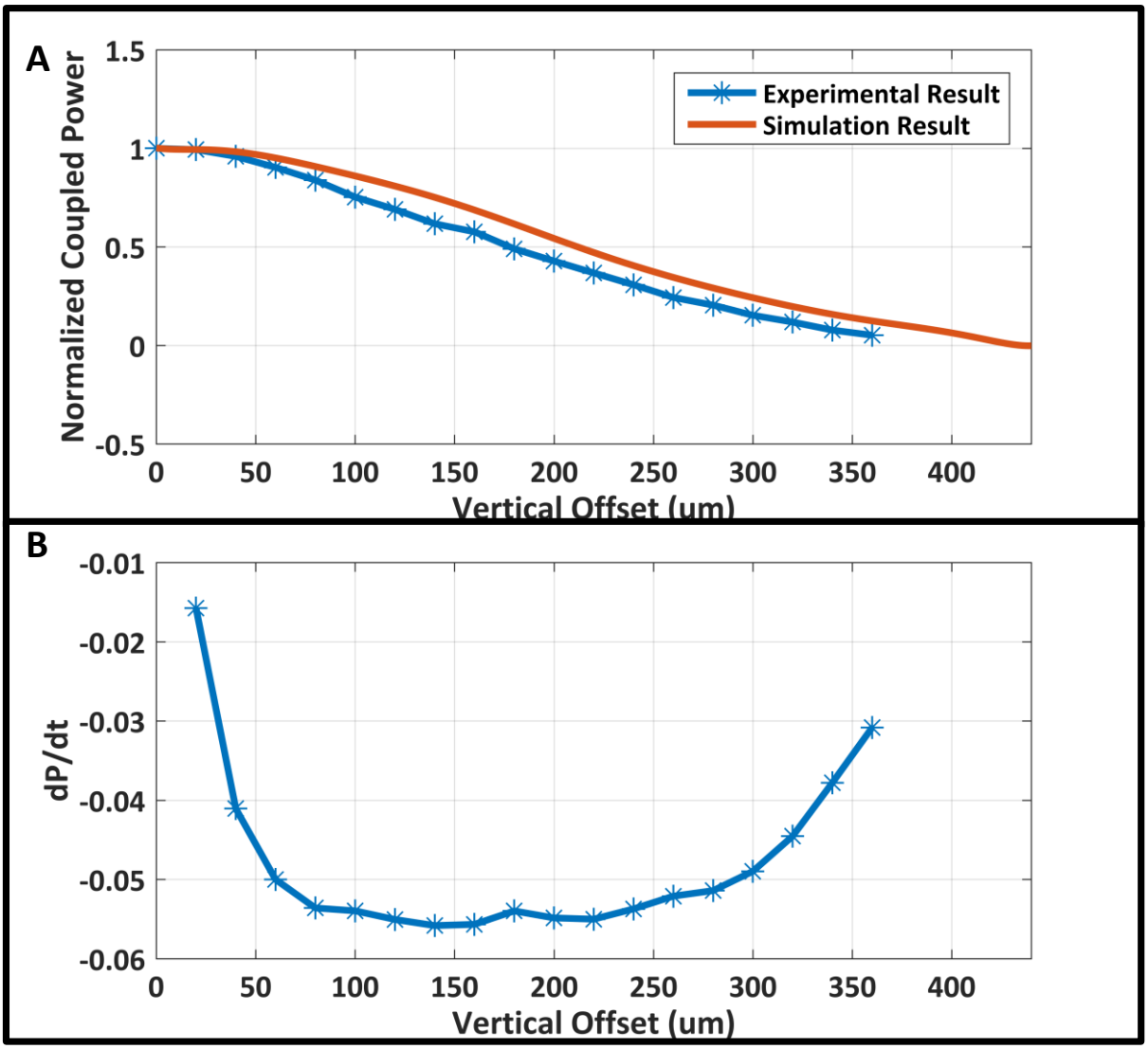

Figure 2.3 a) Normalized power vs offset simulation and experimental data. d = 250 µm, l = 4mm and fiber diameter is 440 µm b) Optical modulation with respect to offset.

2.3 Theory of vibrating cantilever structures

In the proposed sensor system, mechanically resonating optical fibers are deployed. Therefore, it is essential to understand resonant behavior of cantilever beam, in our case cantilever beam has a circular cross section. Resonant characteristic of any cantilever can be expressed by spring constant, resonance frequency and quality factor. Spring constant relates to how stiff the beam is, resonance frequency is a strong function of mass and spring constant. Quality factor includes effect of damping. A simple circularly shaped cantilever is illustrated in figure 2.4.

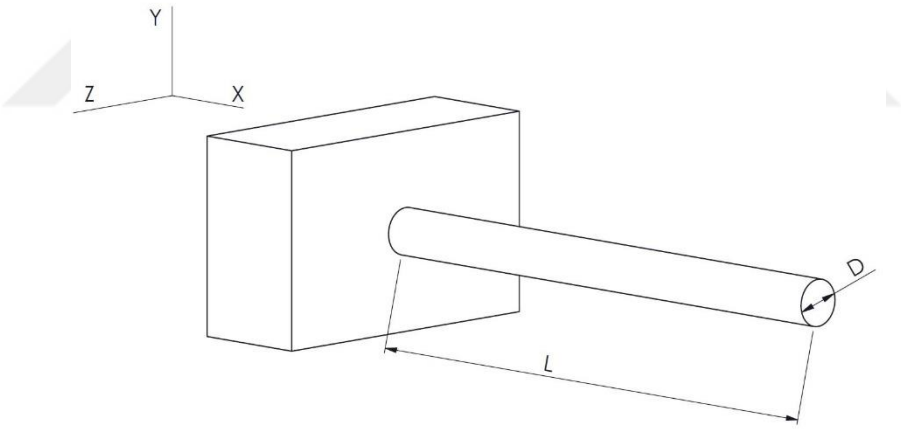

Figure 2.4 Cartoon drawing of a circular cantilever beam

One-dimensional (1D) Euler–Bernoulli equation can be used cantilever beam in order to express time dependent displacement [49]. The Euler-Bernoulli approach is a simple approach to modelling thus it does not include non-linear terms related to large displacement amplitude, rotary inertia or shear deformation.

$$\hat{E}I\frac{\partial^4 w(x,t)}{\partial x^4} + (\rho A + \chi)\frac{\partial^2 w(x,t)}{\partial t^2} + \xi\frac{\partial w(x,t)}{\partial t} = q(x,t) \quad (\mathbf{1})$$

$w(x,t)$ is time varying displacement of the cantilever and $q(x,t)$ is external force function in N/m. $\hat{E}$ is effective Young's modulus of cantilever material. Effective Young's modulus can be expressed as $E/(1-v^2)$ where E is Young's modulus and v is the Poisson ratio. ρ is the specific mass density of the material, A is the cross sectional area, I is the moment of inertia which can be expressed as $\pi d^4/64$ for a uniform circular cantilever beam and ξ is the damping coefficient. Since actuation is remotely done by an electro coil, a nickel part is attached to the fiber. Effect of the nickel part is introduced to the equation by distributed added mass per unit length χ. The added mass χ term also includes effect of particles accelerated by the cantilever which in our case accelerated blood by the movement of the optical fiber.

One-dimensional (1D) Euler–Bernoulli equation **(1)** is a two variable differential equation. The position variable *x* gives the displacement along the beam. The shape of the cantilever beam can also be interpreted by the position variable *x*. On the other hand, the time variable *t* is related with the frequency. Since position variable and time variable are linearly independent to each other, time varying displacement $w(x,t)$ can be separated.

$$w(x,t) = W(x).T(t) \quad (\mathbf{2})$$

Eigen frequency ω_0 can be derived by discarding the external force *(q(x,t)=0)* [110]:

$$\frac{\hat{E}I}{(\rho A+\chi)}\frac{\frac{\partial^4 w(x,t)}{\partial x^4}}{W(x)}=\frac{\xi}{(\rho A+\chi)}\frac{\frac{\partial T(x,t)}{\partial t}}{T(t)}-\frac{\frac{\partial^2 T(x,t)}{\partial t^2}}{T(t)}\equiv\omega_0^2=const \qquad (\mathbf{3})$$

Where *T(t)*, time function, can be expressed as:

$$\frac{d^2T(t)}{dt^2}+\frac{\xi}{(\rho A+\chi)}\frac{dT(t)}{dt}+\omega_0^2T(t)=c \qquad (\mathbf{4})$$

c is a constant. We can express time function as follows,

$$T(t)=Be^{-\gamma t}\sin(\omega_0 t+\varphi) \qquad (\mathbf{5})$$

Then position function becomes,

$$\frac{\hat{E}I}{(\rho A+\chi)}\frac{\partial^4 W(x)}{\partial x^4}-\omega_0^2W(x)=0 \qquad (\mathbf{6})$$

Solution for position function is as follows:

$$W(x)=c_1\cos\left(\frac{\lambda}{L}x\right)+c_2\sin\left(\frac{\lambda}{L}x\right)+c_3\sinh\left(\frac{\lambda}{L}x\right)+c_4\cosh\left(\frac{\lambda}{L}x\right) \qquad (\mathbf{7})$$

We can find the constants coefficients by applying boundary conditions c_1, c_2, c_3, c_4 :

$$W(0) = 0, \qquad \left.\frac{dW(x)}{dx}\right|_{x=0} = 0, \qquad \left.\frac{d^2W(x)}{dx^2}\right|_{x=L} = 0, \qquad \left.\frac{d^3W(x)}{dx^3}\right|_{x=L} = 0 \quad (\mathbf{8})$$

Since one end of the fiber is clamped, displacement and velocity at x=0 is zero. At the free end of the fiber any torsion or bending is excluded. By defining a non-dimensional λ as in 9 a characteristic equation can be written as in (10):

$$\left(\frac{\lambda}{L}\right)^4 = \frac{\rho A \omega_0^2}{\hat{E} I} \qquad (\mathbf{9})$$

$$\cos(\lambda)\cosh(\lambda) + 1 = 0 \qquad (\mathbf{10})$$

λ_a values in (11) are depending on the mode number. The λ values are given as follows for the first four modes [49]:

$$\lambda_1 = 1.875, \quad \lambda_2 = 4.69, \ \lambda_3 = 7.86, \quad \lambda_4 = 11.00 \qquad (\mathbf{11}).$$

Using those λ values, undamped resonance frequency and quality factor of the cantilever beam can be expressed as:

$$\omega_{a,0} = 2\pi f_{a,0} = \frac{\lambda_a^2}{L^2}\sqrt{\frac{\hat{E} I}{\rho A + \chi'}} \qquad (\mathbf{12})$$

$$Q = \frac{\omega(\rho A + \chi)}{\xi} \qquad (\mathbf{13})$$

Whereas damped resonance frequency can be expressed as:

$$\omega_a = \frac{\omega_{a,0}}{\sqrt{1 + \frac{1}{4Q^2}}} \quad (\mathbf{14})$$

Suspended cantilever system can be modelled as a simple mass spring system as shown in figure Figure 2.5:

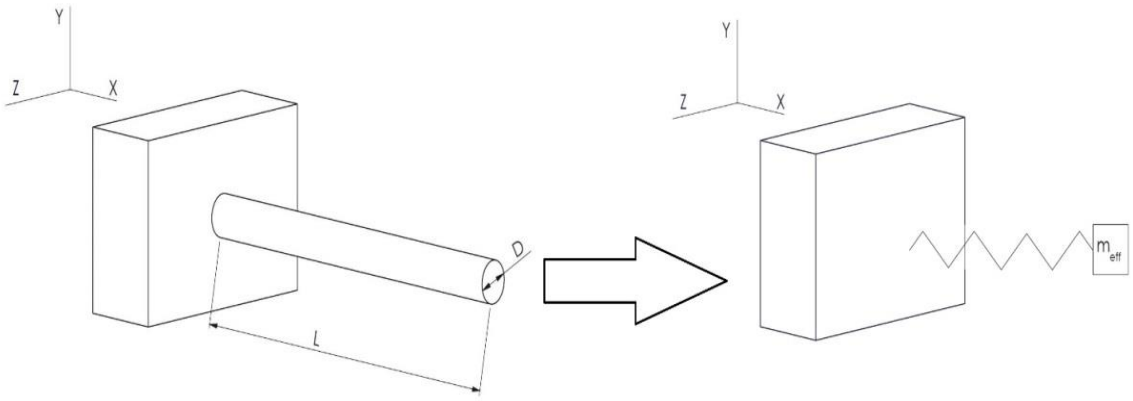

Figure 2.5 Cantilever as a spring-mass system (1D harmonic oscillator)

The resonance frequency of this system is:

$$f = \frac{1}{2\pi}\sqrt{\frac{k}{m_{eff}}} \quad (\mathbf{15})$$

$$k = \frac{3EI}{L^3} \quad (\mathbf{16})$$

$$I = \frac{\pi d^4}{64} \quad (\mathbf{17})$$

$$m_{eff} = m_{eff} = \frac{33}{140}m = \frac{33}{140}\frac{\rho\pi d^2 L}{4} \quad (\mathbf{18})$$

$$f = \frac{1}{2\pi}\sqrt{\frac{3E\frac{\pi d^4}{64}}{\frac{L^3}{\frac{33\rho\pi d^2 L}{560}}}} = \frac{1}{2\pi}\sqrt{\frac{35}{44}\frac{Ed^2}{L^4\rho}} = 0.1419475\frac{d}{L^2}\sqrt{\frac{E}{\rho}} \quad (\mathbf{19})$$

To confirm the mathematical analysis, a simple FEM simulation was done with COMSOL software. Resonant frequency comparison for three different lengths is given in Table 2.1. Cantilever shape of the first mode can be also seen in figure 2.3.

	L[mm]	d[μm]	ρ [kg/m3]	E [GPa]	Analytical[Hz]	Comsol[Hz]	Difference
1	4	440	2200	70	22019	21593	1.93 %
2	6	440	2200	70	9786	9627	1.62 %
3	8	440	2200	70	5505	5421	1.52 %

Table 2.1 Resonance frequency anlasys and Comsol simulation for different length fibers

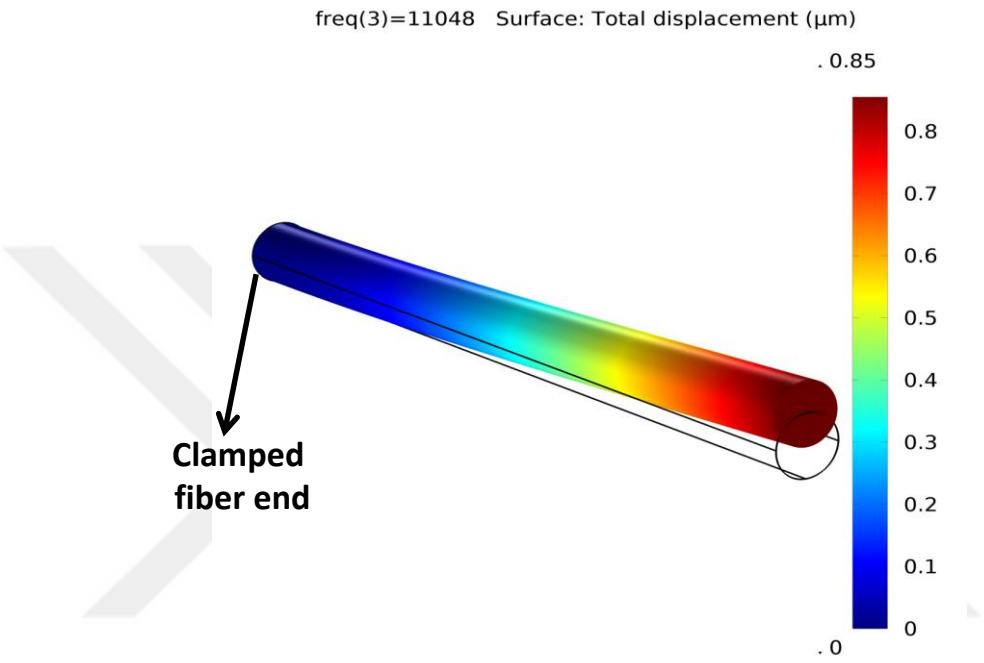

Figure 2.6 Cantilever as a spring-mass system (1D harmonic oscillator)

Cantilever beams in our system are operated in viscous liquid mediums such as blood. A hydrodynamic force per unit length, $f_{hydrodynamic}$ occurs on the cantilever with the presence of viscous liquid medium [36]. This force includes two different terms [50]:

$$f_{hydrodynamic} = -g_1\dot{x} - g_2\ddot{x} \quad (\mathbf{20})$$

x is displacement function of the cantilever beam. The first term is related to viscous drag force and the second term is related to the inertial force related to blood accelerated by the cantilever. Due to complex shape of the cantilever beam and segmented fluid interference caused by fluid stop region proves a challenge to derive mathematical expressions of these hydrodynamic loading terms and it is out of the scope of this thesis study. For further reference, mathematical analysis of hydrodynamic loading for thin rectangular shaped cantilevers can be found in Sader's work [39]–[41].

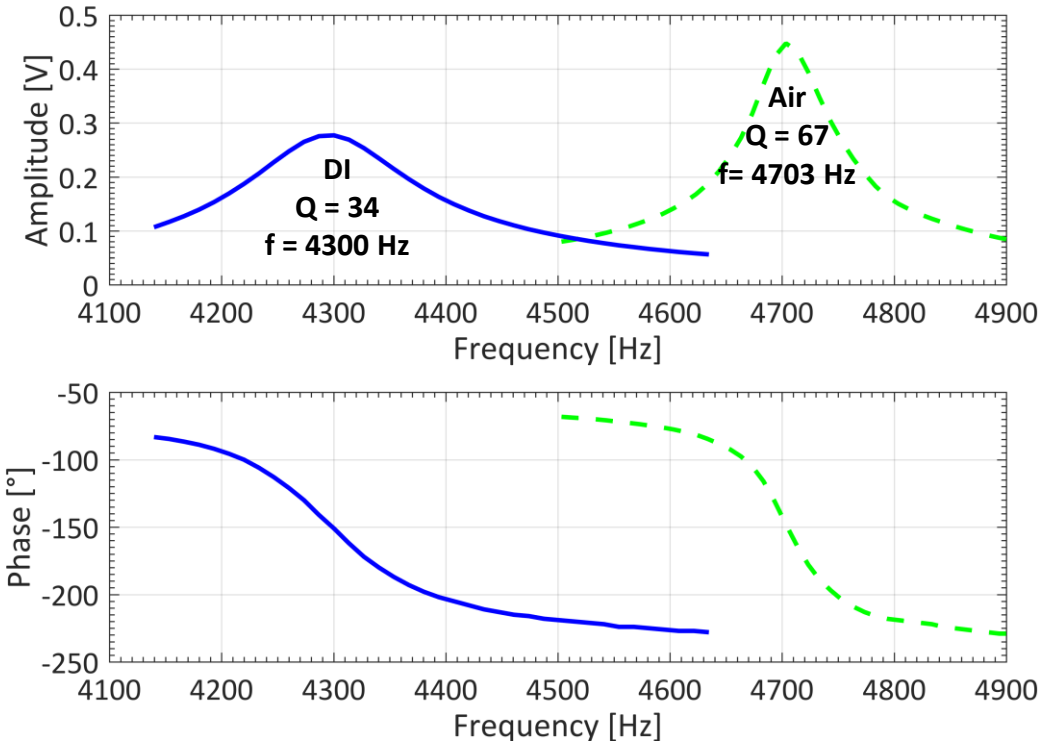

Figure 2.7 Frequency response of the system measured in air and distilled water

Figure 2.7 shows the frequency response of the system for different mediums: air and distilled water (DI). Resonance frequency of the sensor in air is 4703 Hz and quality factor is 67. When distilled water is inserted into microfluidic channel, resonance frequency drops to 4300 Hz and quality factor drops to 34. This change in frequency response is caused by hydrodynamic loading.

2.3 Cartridge Design and Fabrication

In this section, some design issues concerning the cartridge will be discussed firstly, and then the cartridge fabrication will be explained briefly. Cartridge has two main parts; body and two optical fibers. There are two multimode optical fibers in the cartridge with a core diameter of 400 μm and cladding diameter of 440 μm. Body of the cartridge consists of two polymethyl methacrylate (PMMA) parts. Microfluidic channels and grooves are CNC machined into PMMA sheets. Grooves are designed to hold the fibers tightly. Precise machining of these grooves is important because of alignment of the fibers with respect to each other. There are one inlet, one outlet, a sensor chamber and a fluid stop region in the body. Microfluidic channels and inlet geometries are specifically designed to provide fluid flow without pumping or surface functionalization. Thus eliminating extra cost and complexity of pumping and surface functionalization enables more robust, low cost cartridge.

2.2.1 Cartridge Design

Fibers need to be held in appropriate place securely in the cartridge. V grooves are widely used as fiber holders in the industry for precise positioning [51]. V shape allows the fiber to be centered with respect to V shape regardless of fiber size as long as it has excess fiber material over V groove to hold it in place. Figure 2.8 shows fiber placement in V grooves for different fiber sizes. In the proposed platform, cartridges employ perfectly sized V grooves for the suspended fiber and offset V grooves for the receiving fiber. Complementary V grooves, one on the bottom part one on the top part of cartridge, are used for better clamping of the fibers.

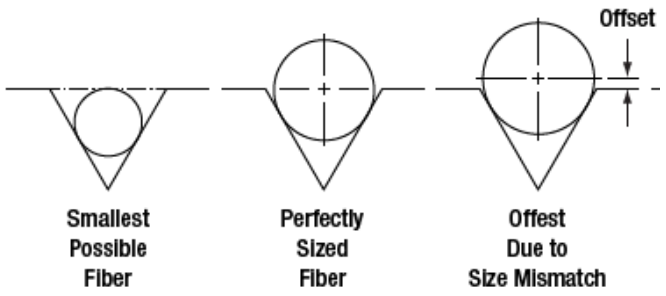

Figure 2.8 Fiber placement in V grooves for different fiber diameters

V groove depths are calculated with basic geometry axioms. Figure 2.9 shows the depth calculation of the perfectly sized V grooves where R is radius of the fiber. For offset V grooves, depth is calculated as $R \pm t$ where t is offset distance from the fiber center. Offset is complementary in the opposing parts of cartridge body. In other words, if V groove offset is 50 µm in one side, in the opposing side offset will be -50 µm. Since we

are using 440 µm fibers, V groove depth is approximately 310 µm. As discussed in section 2.2, offset is set to 120 µm, thus V groove height is 190 µm for bottom part and 430 µm for top part of the cartridge.

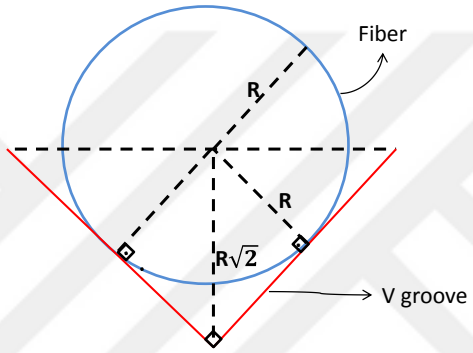

Figure 2.9 Depth calculation of the perfectly sized V grooves where *R* is radius of the fiber

Blood transfer to reaction chamber is provided by microfluidic channels. Blood flow must be self-promoted since any external or integrated pump will increase the system complexity and cost. For point of care systems, cost and simplicity are very important. Blood is introduced to the microfluidic channel through an inlet. Inlet is designed as an angled channel for easy insertion. Microfluidic channels are designed with 800 µm depth and 1 mm width for easy assembly of cartridges. Total volume of blood needed for a successful measurement is around 12 µL which is comparable to state of the art PoC systems. This volume could be further reduced by downsizing the microfluidic channels. In the current design, sizes are kept large for the sake of easy assembly of cartridge.

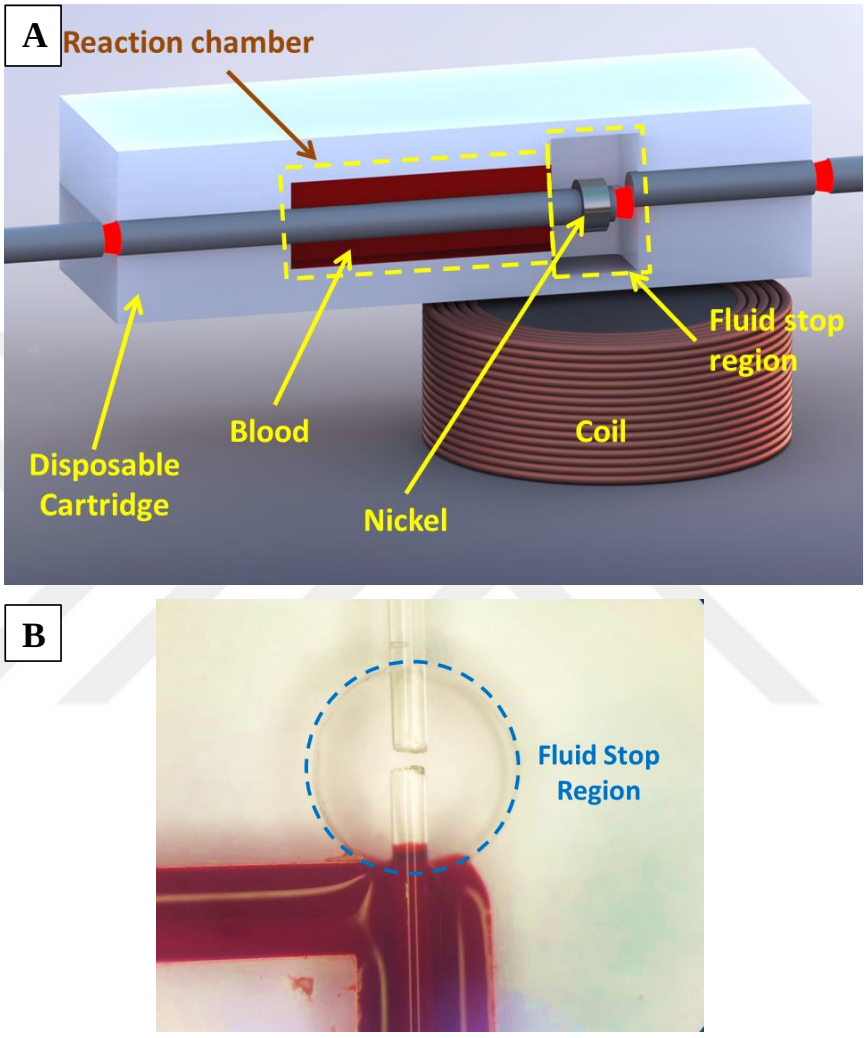

Figure 2.10 Fluid stop region with whole blood flow through micro fluidic channels a) cross sectional view with coil beneath the cartridge (dimensions are not scaled) b) Top view photo of the fluid stop with blood flowing through microfluidic channels

Employing optical read out in blood is challenging because of high absorbent and scattering characteristics of red blood cells [52]. Thus we employed a novel technique

that enables optical read-out in our system with a fluid stop region. Fluid stop region is located where two ends of fiber parts meet each other. Fluid stop region prevents fluid going in between fiber end faces via capillary action. Capillary action is tendency of fluid to flow into smaller gaps rather than larger gaps thanks to adhesion of the liquid to channel walls and cohesion of the liquid at the air-fluid interface. Furthermore, trapped air in the fluid stop aids prevention of leakage of blood in to fluid stop region more. Fluid stop region is machined much larger in terms of both height and width with respect to sensor chamber. Figure 2.10 shows fluid stop region with blood flow. In our cartridges, sensor chamber is machined to 800 μm depth and 1 mm width whereas fluid stop region was machined to 1.6 mm height and 2 mm width. Since blood flow inside the cartridge is promoted by capillary motion too, a possible forced flow into fluid stop region is prevented. Preventing light going through blood by employing a fluid stop region enables a robust optical read out scheme.

2.2.2 Cartridge Fabrication

Cartridges were fabricated in house with off the shelf materials. There are three main steps to cartridge fabrication; machining of PMMA sheets, nickel attachment to vibrating fiber and assembly of the cartridge. Cartridge design can be seen in figure 2.11.

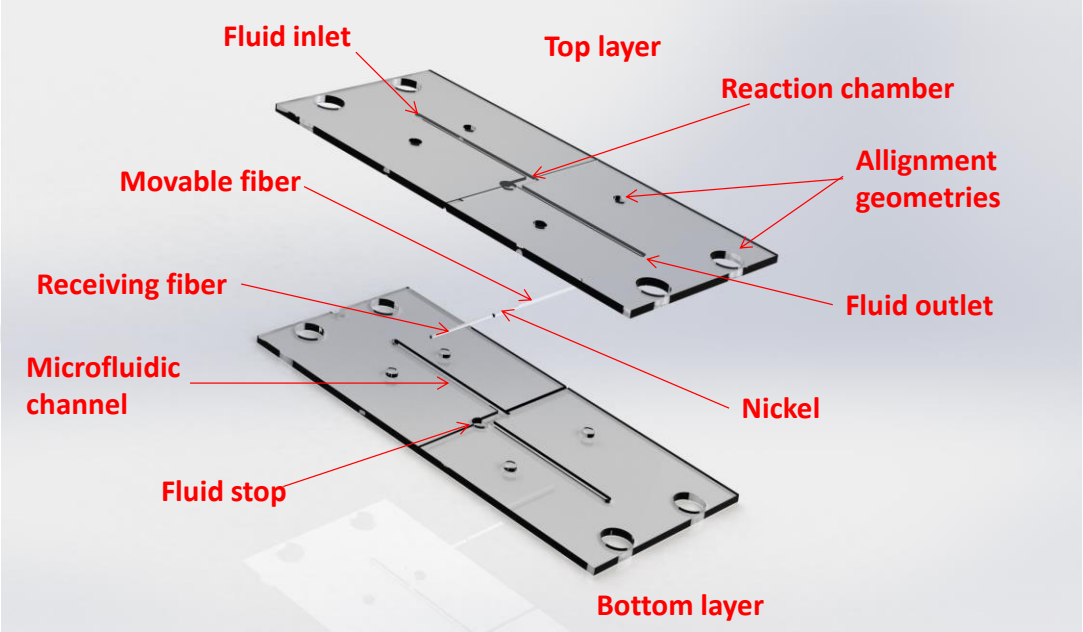

Figure 2.11 Exploded view of cartridge

As Computer Numerical Control (CNC) tools have become more precise and affordable in the last decade, CNC tools become a versatile tool for fast prototyping of microfluidics in the recent years [53]. CNC tools offers precision of micron scale with no initial cost except machine set-up. We have been using a five axis CNC from MDA Precision, US. This CNC is capable of a spindle rate of 60000 RPM which becomes important when small diameter (for example 100 µm) cutting tools [54]. CNC machine was calibrated before micromachining and we were able to machine microfluidic channels with 80 µm depth with an accuracy of ±4 µm using 1 mm diameter flat endmills. First, cartridges were designed using a Computer Aided Design (CAD) tool, Solidworks. Then g-codes were generated for micromachining using Computer Aided Manufacturing (CAM) tool, Inventor. V grooves were machined by tilting the cutting tool by 45^{o} as

shown in figure 2.12.b. This allows machining of small size V grooves without need of a high precision V shaped cutting tool. V grooves were able to be machined as small as 20 µm using 1mm diameter flat end mill as long as tool tip has has sharp corners. It is a very powerful technique indeed since small sized microfluidic channels can be machined without need for expensive CNC machines with high RPM spindle rates and small diameter cutting tools.

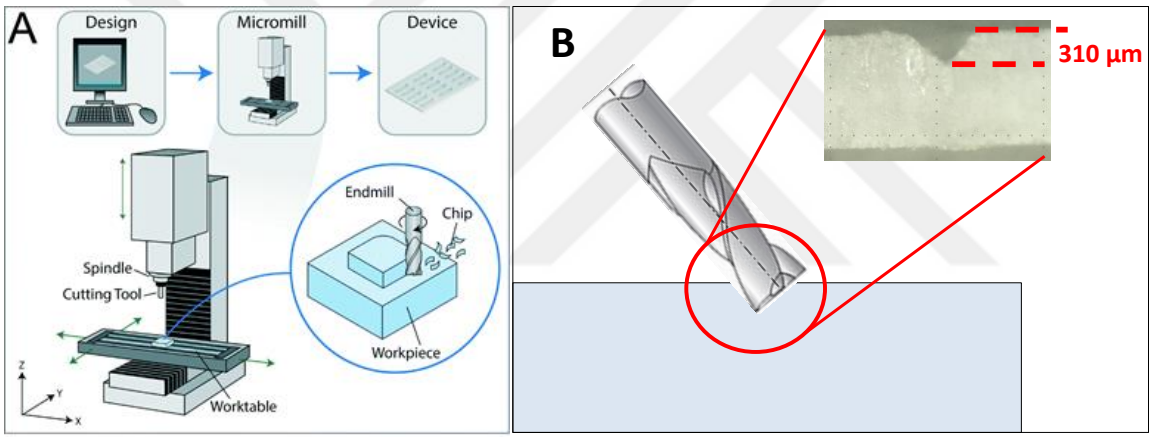

Figure 2.12 a) Micro milling process: cartridges is designed using a Computer Aided Design (CAD) tool, g-code is generated using Computer Aided Manufacturing (CAM) tool, cartridges are fabricated with CNC machine b) V groove machining by tilting the cutting tool by 45^{o}

PMMA was chosen as cartridge material. PMMA is clear, suitable for micro machining and biocompatible [55]. 2 mm thick PMMA sheets were purchased in large sizes and cut down to CNC compatible size (10cm by 10cm) with a CO_2 laser cutter. PMMA sheets are attached to CNC vise via a custom made vacuum holder.

A ferromagnetic volume is needed for electro-magnetic actuation. In this work, nickel was used for this purpose. Prior to nickel attachment, fibers are stripped and cleaved to length. Two methods were employed for nickel attachment: coating and attachment by bonding. Coating was done as follows: Thin (50 nm) Ti layer for better adhesion to fiber was deposited followed by a seed Ni layer (100nm) by a RF sputter. Then 10 μm Ni was deposited using a electro plating set-up. SEM image of a Ni coated fiber can be seen in figure 2.13.a. As Ni coating becomes thicker, force applied will increase but stiffness of the fiber also increase since Ni is very stiff compared to glass. Therefore, putting Ni at the tip rather than coating all fiber surface area is more efficient instead of thick coating. This way, torque is increased since all magnetic force is applied at the tip without adding any stiffness to fiber. Moreover, coating tip of the fiber with a thick layer of Ni is challenging. Therefore, a nickel wire was cut to length (1 mm long 350 μm diameter) and attached to fiber tip with using low viscosity super glue (Pattex Sekundenkleber Plastix Flüssig, Germany). Microscope image of Nickel attached fiber can be seen in figure 2.13.c. Glued nickel part makes magnetic actuation possible for electro coil. Clean room processes are not needed for the sensor fabrication which reduces cost and build time significantly.

PMMA parts were bonded by either using epoxy or thermal compression bonding. Fibers are placed onto V grooves and temporarily fixed with 10% PVA solution. Single channel cartridges were bonded using optical grade UV curable epoxy (NOA 81, Norland Products US). NOA 81 is low shrinkage and fast curing thus enabling precise cartridge dimensions. PMMA parts are held in place with clamps and epoxy is wicked from sides. Epoxy flows between PMMA layers by capillary motion and stops at the edges of

microfluidic channels, similar to fluid stop. Then epoxy is cured in a custom made UV chamber immediately.

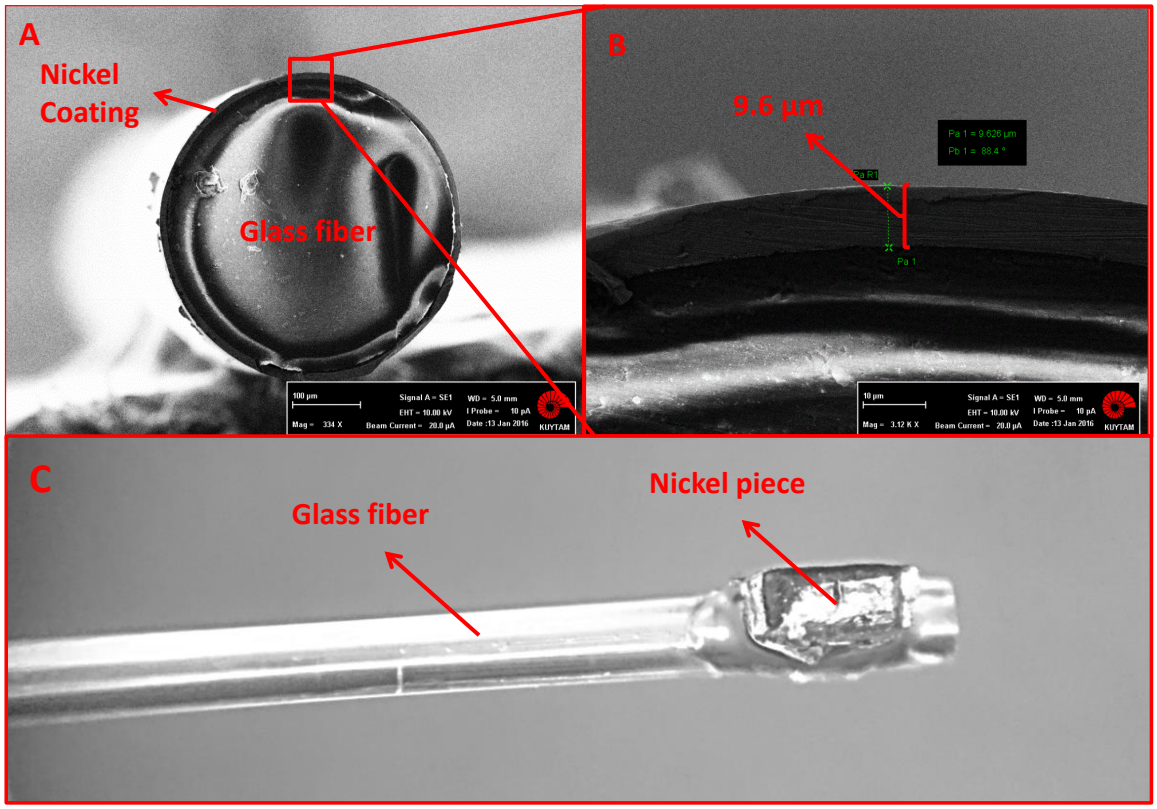

Figure 2.13 a) SEM image of Nickel coated fiber b) SEM image focused on the Nickel coating with a thickness of 9.6 µm. c) Microscope image of Nickel attached fiber

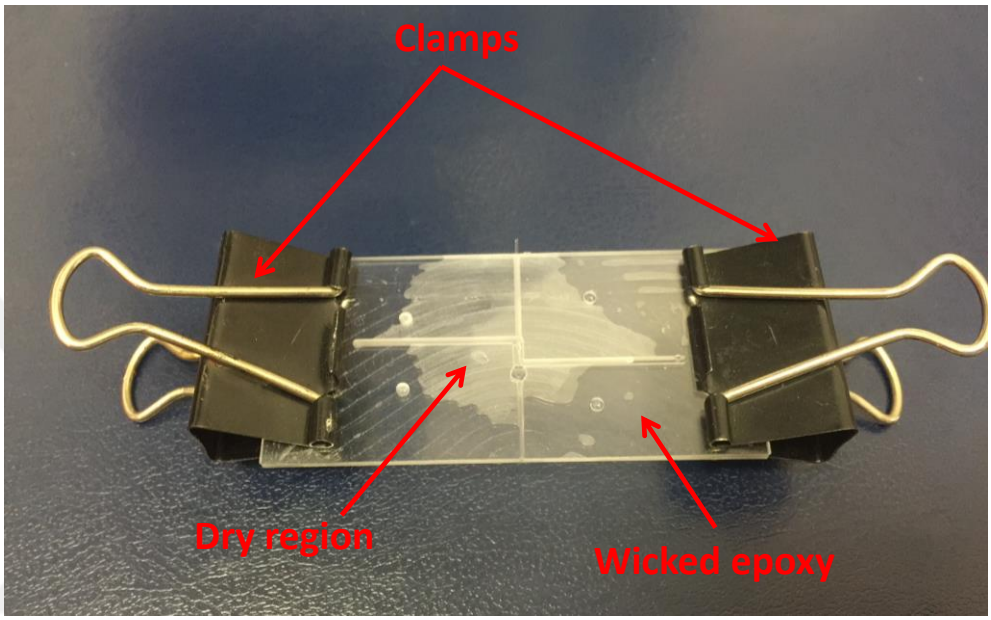

Figure 2.14 Epoxy bonding by wicking

Multichannel designs cannot be assembled with epoxy due to complexity of cartridge. A custom made thermal compression rig was built and used for multichannel cartridge assembly as shown in figure 2.15. PMMA sheets are heated to glass transition temperature (92^{o}C for the specific PMMA used) and bonded by applying high pressure. Amount of pressure is adjusted with an adjustable torque wrench. Temperature is controlled with an controller and sheets are heated by aluminum slabs with embedded heating wires. More detailed information on thermal compression bonding can be found in [56].

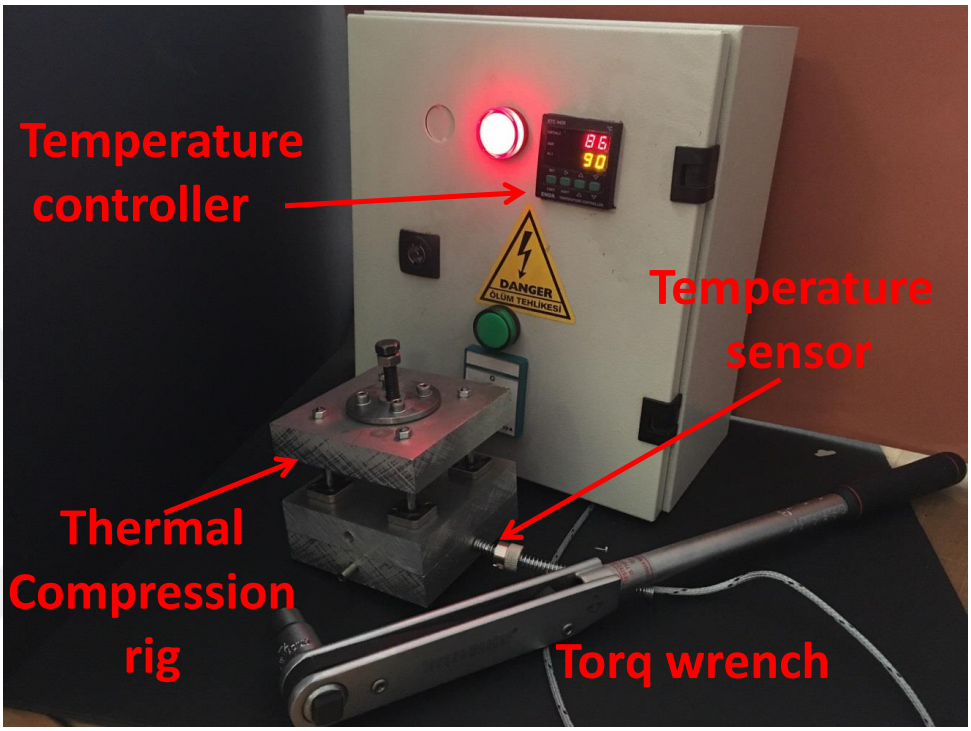

Figure 2.15 Custom made thermal compression set-up. Temperature is controlled by a temperature controller, precise pressure is set with a torque wrench

2.4 Measurement Set-up

In this section, details of the measurement set-up used for results reported in the Chapter 3 are given. Specification of each building block including magnetic actuation, optical read out, electronic read out and temperature control is discussed in component level. Measurement set-up can be seen in figure 2.16. Coupling fibers are aligned to cartridges by micrometer translation stages. Cartridge is clamped onto an aluminum fixture for mechanical stability.

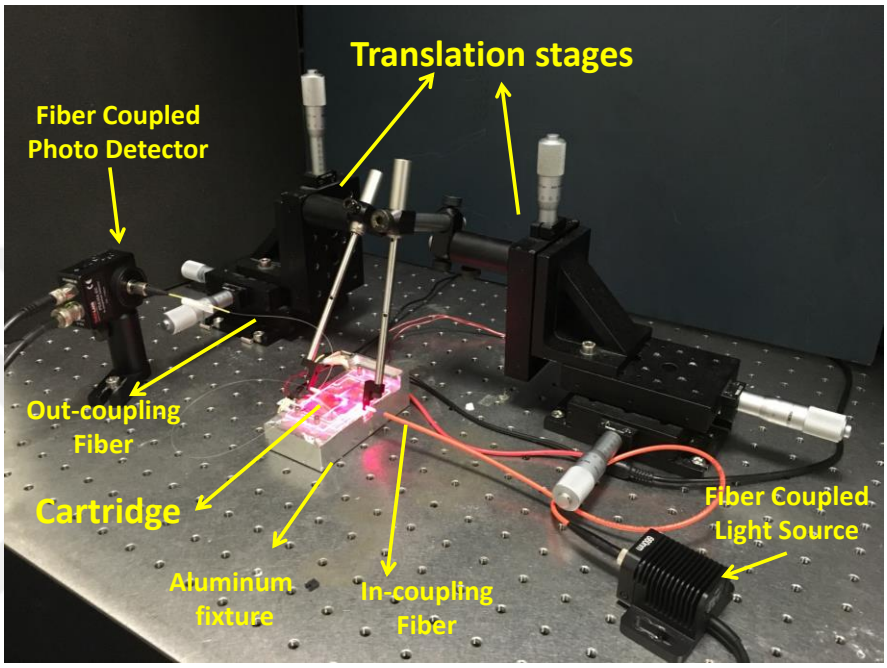

Figure 2.16 Photo of measurement set-up

2.2.1 Magnetic actuation

Remote actuation is vital for in liquid operation, especially for point of care application where disposable cartridges are used [57]. Remote actuation can be achieved by magnetic, thermal-optic, electro-static methods. Thermal-optical actuation needs tight alignment tolerances with the actuation beam and absorbent material on the cantilever whereas electro static method is not an option due to large gap between the cartridge face and cantilever. The optical fibers are remotely actuated by a electro coil attached embedded inside the aluminum holder. A cylindrical shaped neodymium permanent magnet is placed inside the electro coil for DC magnetic biasing (0.45 T at the location of nickel part). If nickel part attached to the optical fiber is not magnetized, then electro coil

will only pull the nickel part and release it without any repelling action. Therefore, it is essential to magnetize the nickel part along the B field of coil. [117]. Coil is constructed by 0.3 mm diameter copper wires coiled around the cylindrical permanent magnet with a turn number of 80. The total diameter and height of this custom made coil is 14 mm and 8 mm respectively figure 2.17.

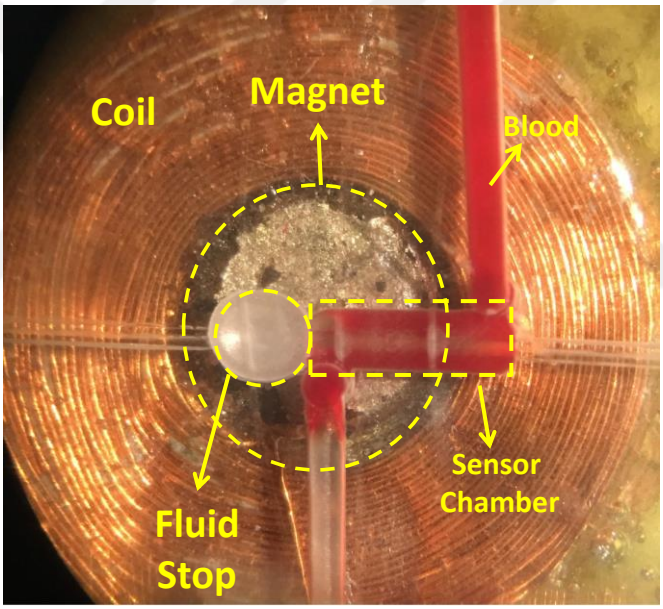

Figure 2.17 Photo electro-coil with cartridge. Sensor is placed on top of permanent magnet

The coil is driven with a custom designed high power broadband current amplifier. This driver is capable of operating in between DC to 30 kHz frequency range. B field generated at the fiber location is around 2 mT. Figure 2.18 shows the fiber displacement for a 440 µm diameter 6 mm long fiber with 350 µm diameter 1 mm long

nickel wire attached to the tip. Displacement measurements were taken with a Laser Doppler Vibrometer (LDV). LDV exploits the Doppler shift and detects the vibration of a surface remotely. Laser Doppler Vibrometer (Polytec: 3.4 MHz Laser Doppler Vibrometer) with a controller unit (OFV-5000 Modular Vibrometer Controller) is used in this work.

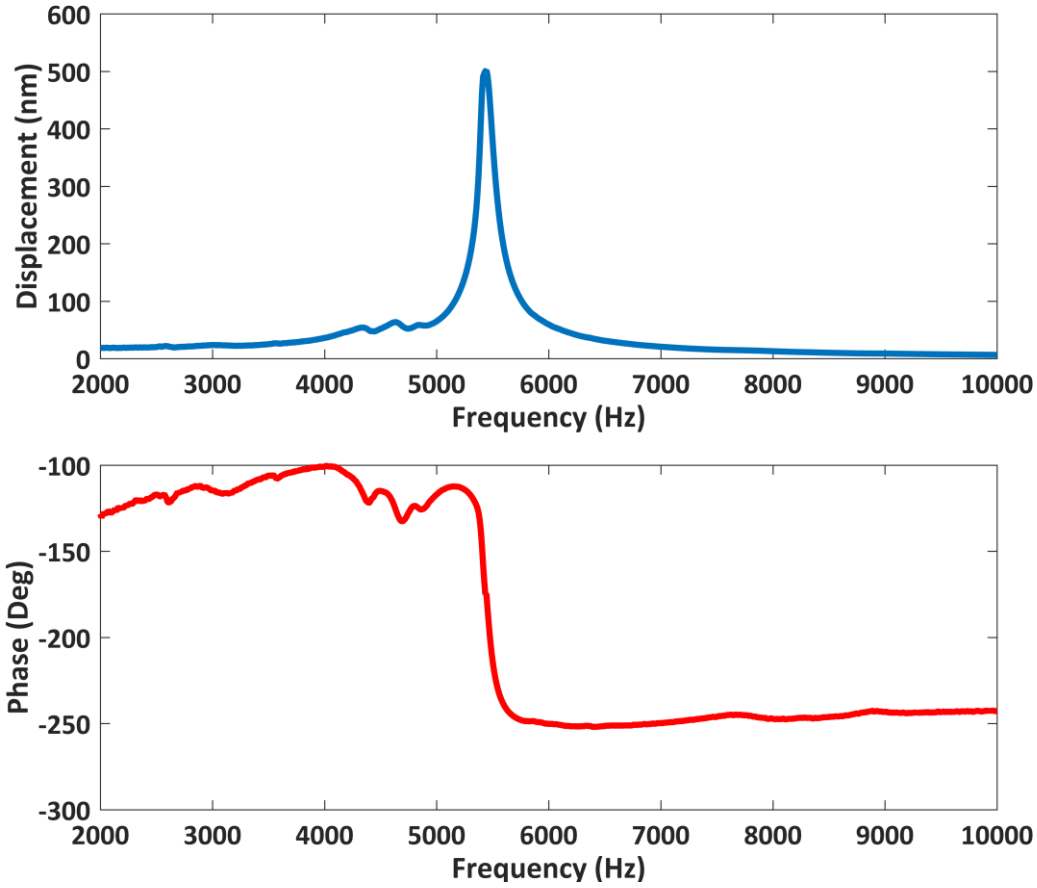

Figure 2.18 LDV measurement showing resonance characteristics of the system with a maximum displacement of 520 nm in air operation

2.2.2 Optical Read-out

As previously mentioned, cartridge without electrical connection is important for point of care application for the sake of simplicity, cost and robustness. Therefore, we used an optical read out scheme. Detailed discussion of the optical sensor has done in Section 2.3. A fiber coupled LED, Thorlabs M660F1, was used with a 400 μm core multimode in-coupling optical fiber. LED has a wavelength of 660nm for a possible fully blood immersed operation since 660nm is the spectral window for whole blood [52]. LED source provides an optical output power of 14.5 mW when coupled to 400 μm core multimode fiber. Out coupling fiber was selected 105 μm core multimode fiber for better alignment tolerance and cladding mode noise which was explained in detail in Appendix C. Out coupling fiber is connected to a Si photo detector with a variable gain amplifier (Thorlabs PD36A). Gain of the photo detector is adjusted with respect to DC optical power level so that photo detector is not saturated. Coupling fibers were aligned to cartridge with precision translation stages.

2.2.3 Electronic Read-out

Hydrodynamic loading due to coagulation can be tracked through either frequency tracking or amplitude and phase tracking at fixed frequency. Frequency change can be traced with a Phase Lock Loop (PLL) control system. PLL system generates a signal whose phase is constant to reference signal. As phase of the reference signal changes, PLL tries to keep phase constant and adjust the driving frequency accordingly. On the other hand, when system is driven at a fixed frequency, a change will happen in amplitude and phase at that fixed frequency as resonance characteristic of the system

changes. Figure 2.19.a shows frequency response change during coagulation. In uncoagulated plasma, resonance frequency was 4214 Hz and quality factor was 29 whereas after coagulation resonance frequency and quality factor dropped to 4191 Hz and 22 respectively. Change in resonance frequency is not very large but change in amplitude and phase response of the system is significant. Therefore, tracking amplitude and phase rather than frequency change gives better results.

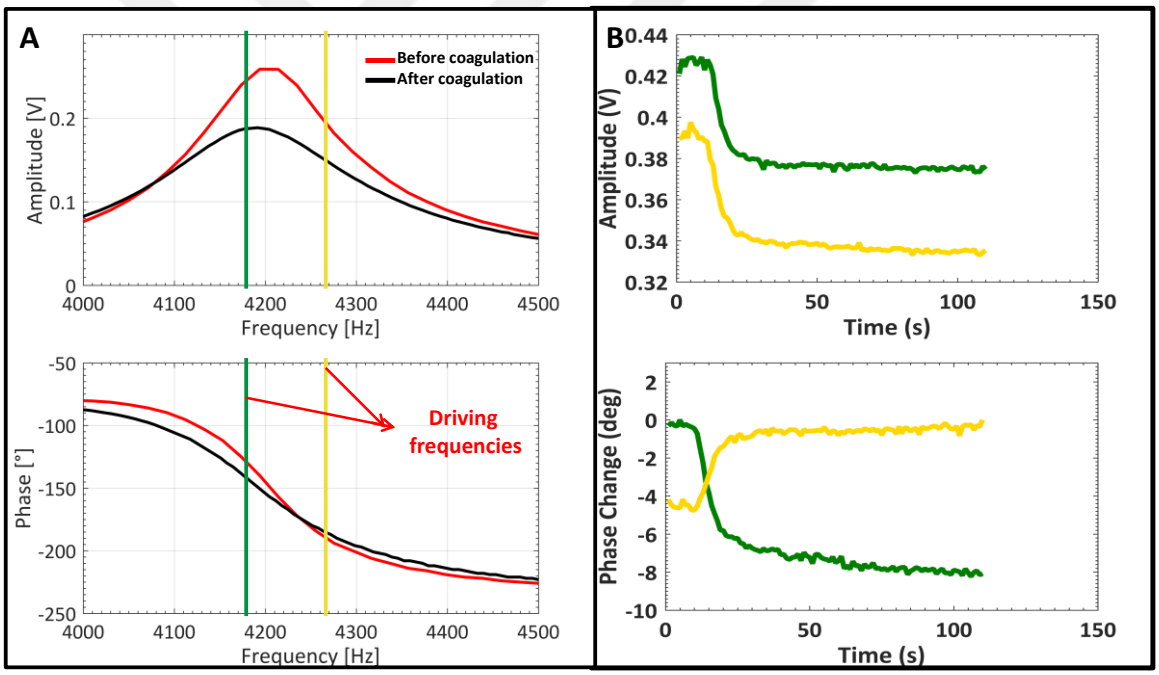

Figure 2.19 a) Frequency response of coagulated and uncoagulated plasma: resonance frequency changed from 4214 Hz to 4191 Hz and quality factor changed from 29 to 22. b) Phase and amplitude change at two different excitation frequency.

Electronic read out block is based around a lock-in amplifier. Lock-in amplifiers enable phase and amplitude measurement of low signal to noise ratio (SNR) signals.

Amount of amplitude and phase change is different for individual excitation frequency. As can be seen from figure 2.19.a, around resonance frequency amplitude change is maximum whereas phase change is minimum. While phase decreases on the left hand side of the resonance frequency when coagulation happens, phase increases on the right hand side of the resonance frequency. Figure 2.19.b shows amplitude and phase change during coagulation for two different excitation frequency. Coil was driven with two different frequencies consecutively for short time periods. Amplitude and phase data of two excitation frequencies was collected as a single data stream. Individual data sets were extracted by post processing. Note that cartridge used for frequency response shown in the figure 2.19.a is different from cartridge used for multi frequency excitation due to timing constraint of frequency sweep. Green and yellow bars are tentatively placed on the frequency response graph for demonstration purposes since all cartridges show similar frequency responses.

Amplitude change is maximum when amplitude level is maximum thus results in a high SNR signal. Phase change is maximum away from the resonance frequency, meaning amplitude level is low when phase change is high thus results in a lower SNR signal. Amplitude change was monitored during all coagulation measurements due to higher SNR value. Phase change can be monitored too. However, it is not straight forward to determine the driving frequency.

2.2.4 Temperature Control

Precise temperature control is very important during coagulation time measurements since coagulation time strongly depends on temperature. aPTT time is more tolerant to temperature changes around 37^{o}C. aPTT clotting time changes approximately 1.5 s/^{o}C above 37^{o}C and 5s/^{o}C below 37^{o}C [58]. Temperature controller used in the set-up is capable of maintaining the temperature of cartridge and fixture at 37±0.1 ^{o}C.

3 COAGULATION MEASUREMENTS

In the previous chapter, working principles of the proposed system were discussed in detail and fabrication process for cartridges was given. In this chapter, proposed platform will be demonstrated through several coagulation tests. Firstly, system was characterized for different mediums. For further characterization, aPTT tests were conducted with three different control plasmas. Subsequently, whole blood aPTT capability was demonstrated using the sensor platform.

3.1 System Characterization

System was characterized in different mediums before the coagulation tests. Frequency sweeps were conducted in air, distilled water, uncoagulated plasma and 3 minutes old coagulated plasma. Figure 3.1 shows the frequency response of the system for different mediums. Resonance frequency of the sensor in air is 4703 Hz and quality factor is 62. When distilled water is injected into microfluidic channel, resonance frequency drops to 4300 Hz and quality factor drops to 34. This change in frequency response is caused by hydrodynamic loading.

Frequency sweeps were done before coagulation of control plasma and 3 minutes after coagulation. Similar to air and distilled water test, both resonance frequency and quality factor decreased. In uncoagulated plasma, resonance frequency was 4214 Hz and quality factor was 29 whereas after coagulation resonance frequency and quality factor

dropped to 4191 Hz and 22. Change in resonance frequency is not very large but change in amplitude and phase response of the system is significant.

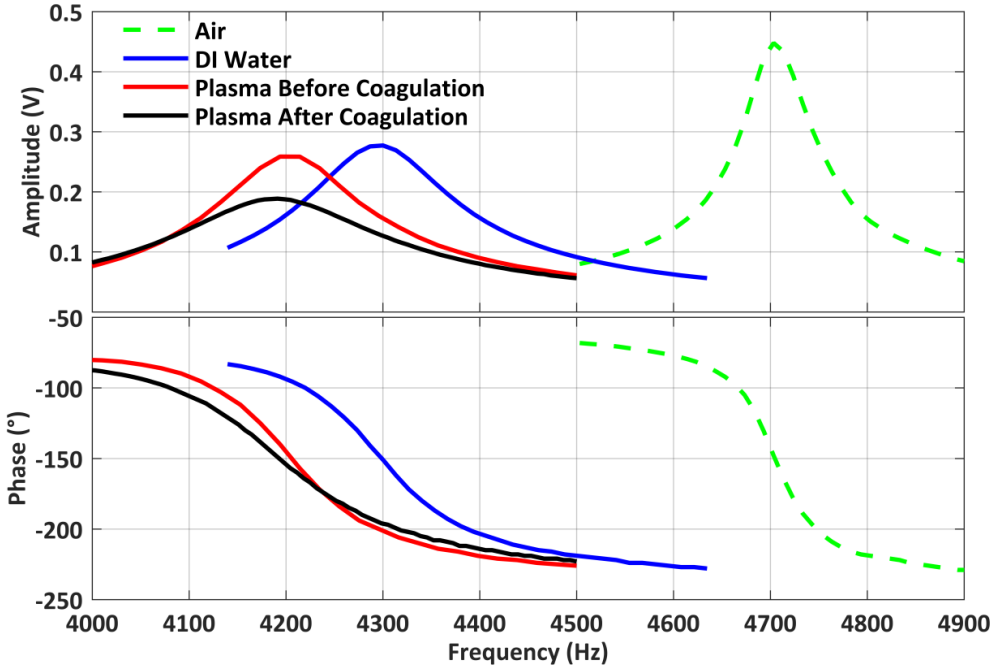

Figure 3.1 Frequency response of the system to air, distilled water, uncoagulated blood plasma and blood plasma after coagulation

As can be seen in figure 3.1, amount of change for amplitude and phase are different for particular frequency in which system is driven. For instance, decrease in amplitude is at maximum at around 4200 Hz whereas change in phase is at maximum at around 4120 Hz and 4350 Hz. Moreover, phase can decrease or increase depending on the particular frequency whereas amplitude only decreases due to increased viscous drag. Since proposed system is more sensitive in amplitude response according to characterization tests, measurements were conducted at a fixed frequency around

resonance frequency of uncoagulated plasma where amplitude change is at maximum and amplitude response was monitored. In other words, input signal for coil was selected as resonant frequency of the fibers in uncoagulated medium.

Blood coagulation times are usually measured with either PT or aPTT test protocols. PT tests are used for measuring potential defect in extrinsic fibrinogen generation pathway whereas aPTT tests are used for measuring potential defect in intrinsic fibrinogen generation pathway. PT test times usually takes 15 seconds where aPTT test times usually takes significantly longer time around 35-40 seconds [63]. Even with a severe abnormality, aPTT tests do not exceed 120 seconds. Figure 3.2 shows long term stability of the system in distilled water for 10 minutes which is more than 5 times the aPTT times of severely abnormal blood samples. Therefore 10 minutes of stability is sufficient for PT and aPTT applications. Stability measurement yielded a standard deviation of 1.2 mV over 734mV signal and a standard deviation of 0.35^{o} in phase difference between drive signal and read out signal in distilled water. Standard deviation of stability data can be interpreted as noise floor of system. Signal to Noise Ratio (SNR) is used in determining signal quality and sensor sensitivity of a system. SNR is, as name implies, ratio of the signal power to noise power. In our system, since noise and signal are measured from a photo detector, output signal is in amplitude. Therefore SNR of the system is calculated 612 by taking the standard deviation of 1.2mV as noise floor of the system using formula (21).

$$SNR = \frac{Psignal}{Pnoise} \qquad (\mathbf{21})$$

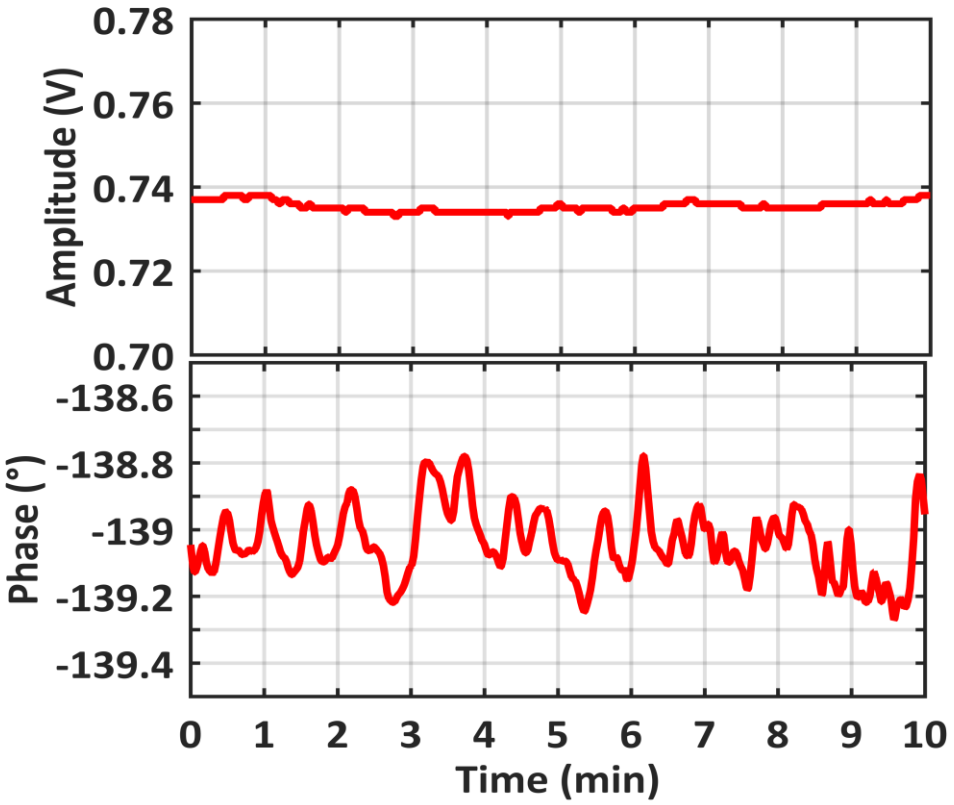

Figure 3.2 Stability results of distilled water for 10 minutes. Amplitude has a 0.16 %RSD and phase has 0.35^{o} standard deviation

3.2 aPTT tests with Control plasma

In the scope of this report, aPTT tests were conducted by using the proposed system with control plasma. We used three different control plasma samples; normal (DIAGEN, UK, lot no: KP93), abnormal 1 (DIAGEN, UK, lot no: AB1-80) and abnormal 2 (DIAGEN, UK, lot no: AB2-79). While normal control plasma samples have coagulation times similar to a healthy person's, abnormal 1 samples have mild abnormality in

coagulation time whereas abnormal 2 have severe abnormality. Each test was repeated 3 times in order to investigate reproducibility of the system. Measurement results were compared to manufacturer datasheet for performance evaluation of the system. Results can be seen in Table 3.1.

3.2.1 Test protocol

- **STEP 1:** Set the temperature of the setup to 37^{o}C and wait 30 minutes to settle
- **STEP 2:** Heat a water bath to 40^{o}C
- **STEP 3:** Mix control plasma powders with distilled water according to manufacturer datasheet
- **STEP 4:** Place the plasma samples, Micronised Silica/Platelet Substitute Mixture reagent and 25 mM CaCl2 in the heated water bath and wait at least 5 minutes
- **STEP 5:** Place cartridge onto holder. Wait 5 minutes to ensure cartridge is at 37 oC.
- **STEP 6:** Adjust in coupling and out coupling fibers for maximum DC signal using translation stages.
- **STEP 7:** Adjust PD gain and pre-amp gain accordingly. Do a wide enough frequency sweep before injecting any liquid into microchannels.
- **STEP 8:** Mix the 50 μL of reagent and the 50 μL of plasma sample in an 500 μL Eppendorf tube and wait for 5 minutes for incubation. Ensure the perfect mixing by occasional tilting.
- **STEP 9:** Mix the control plasma/Micronised Silica/Platelet Substitute Mixture reagent solution with 50 μl of the 25 mM $CaCl_2$. Ensure the perfect mixing with gently pipetting 3 times. Immediately start the clock (t=0)

- **STEP 10:** Immediately place the 50 μL of the mixture into cartridge
- **STEP 11:** Do a very fast crude frequency sweep and find approximate resonance frequency. (Drive coil at that frequency and start recording amplitude and phase difference between the coil input and sensor output. Note the time on the stop watch. (The frequency doesn't need to be the exact peak resonance frequency)

STEP 12: Check the remaining sample in the Eppendorf tube by gently pipetting for fibrin formation. Check the remaining mixture in the Eppendorf tube by gently pipetting for fibrin formation. Note the time on the stop watch when pipet is clogged or fibrin formation is observed.

- **STEP 13:** Monitor the sharp phase and amplitude change and record data for 180 more seconds after stabilization.
- **STEP 14:** Do a wide enough frequency sweep exactly 180 seconds after coagulation
- **STEP 15:** Remove the used cartridge from the cartridge and throw it to the medical waste bin.
- **STEP 16:** Repeat STEP 3-15 until all cartridges are tested.
- **STEP 17:** Turn off all the equipment and throw all non-usable biologic samples to medical waste bin.
- **STEP 18:** Save amplitude and phase data. Extract the first part of the data where sample insertion occurs for better assessment of the coagulation.
- **STEP 19:** Observe the amplitude drop where coagulation happens. Fit a polynomial curve to amplitude data around this drop and take first derivative of the polynomial fit. Local minimum of the signal is coagulation time.

3.2.2 Results

The amplitude and phase response of the system for aPTT test from control plasma can be seen in figure 3.3. A sudden decrease in both amplitude and phase is observed around 48 seconds due to clotting. Since driving signal was optimized for maximum amplitude sensitivity, phase change is less tangible. Circular cross-section shape of the optical fiber has significantly less drag coefficient compared to flat surface of conventional cantilevers that are used in biosensor applications [36]. More aerodynamic structure shape results in less drag force applied by the viscous medium. Therefore, mechanical displacement of vibrating optical fiber based cantilevers is less sensitive to viscosity change. However, optical read-out scheme presented in this report is very sensitive to mechanical displacement which results in high amplitude electrical read out amplitude.

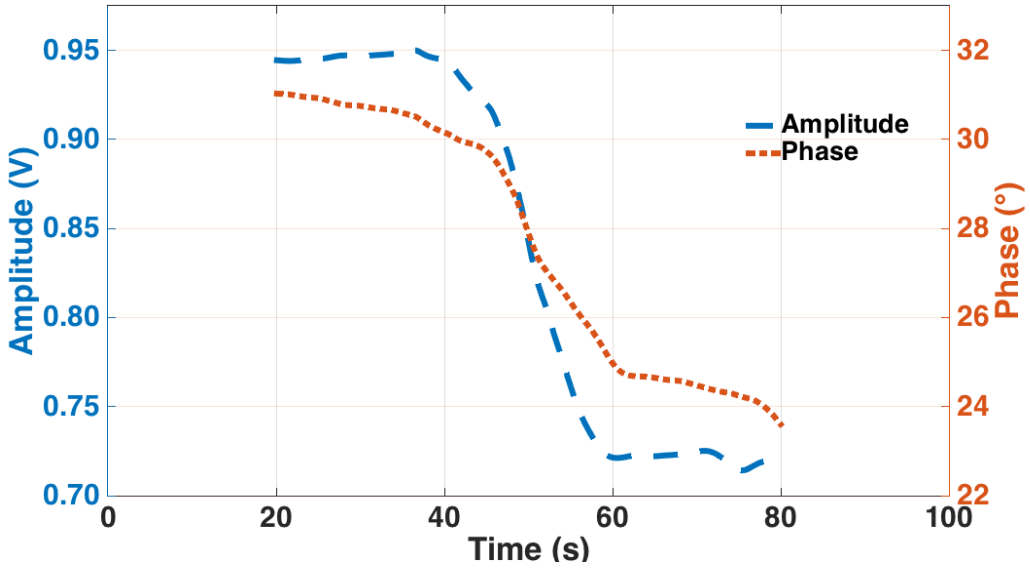

Figure 3.3 Amplitude and phase change during coagulation of abnormal 1 control plasma.

Determining exact time of the coagulation is very important. Amplitude and phase drop due to coagulation is observed over a time period of more than 10 seconds in the system. Discussion on coagulation curve interpretation can be found in Appendix A. Briefly, a polynomial was fitted to amplitude data and first derivative of this polynomial was taken. In figure 3.4, raw amplitude data, polynomial fitted data and first derivative of the polynomial fit is shown. There are two important points in the derivative data. First one is where the derivative is zero which can be interpreted as start of coagulation. Second one is the local minima of the derivative which can be interpreted as mid-point of the coagulation.

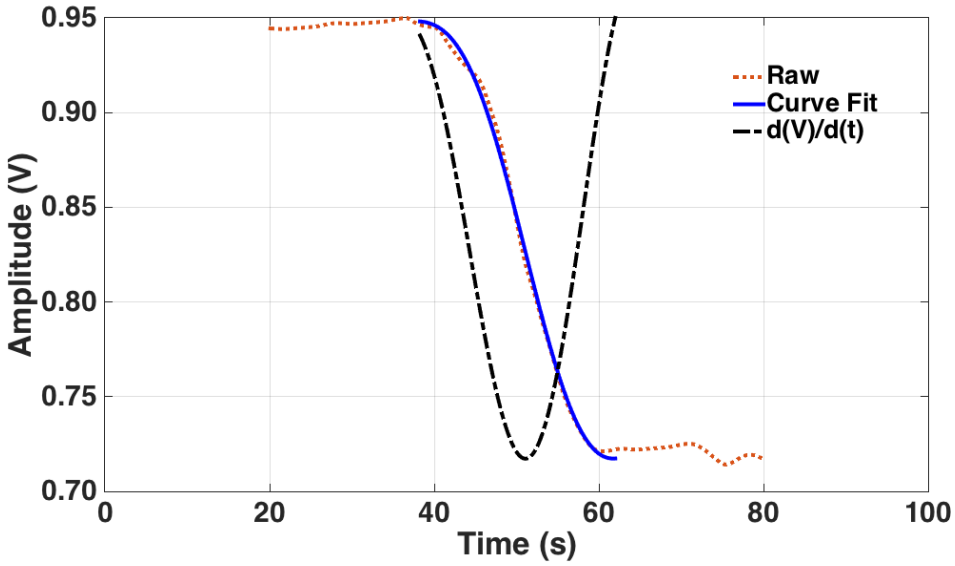

Figure 3.4 Polynomial fit to amplitude and its first derivative. Time of local minimum of the derivative is reported as coagulation times.

Since local minima well overlaps with both manufacturer data sheet [63] and control samples that were observed by pipetting, local minima time of the first derivate was used for quantitative coagulation times. Figure 3.5 shows measurement results and their derivative for normal, abnormal 1 and abnormal 2 control plasma samples (n=3 for each test). As can be seen for the figure 3.5, even though the amplitude responses shows slight different trends, local minimums of the amplitudes closely overlaps with each other.

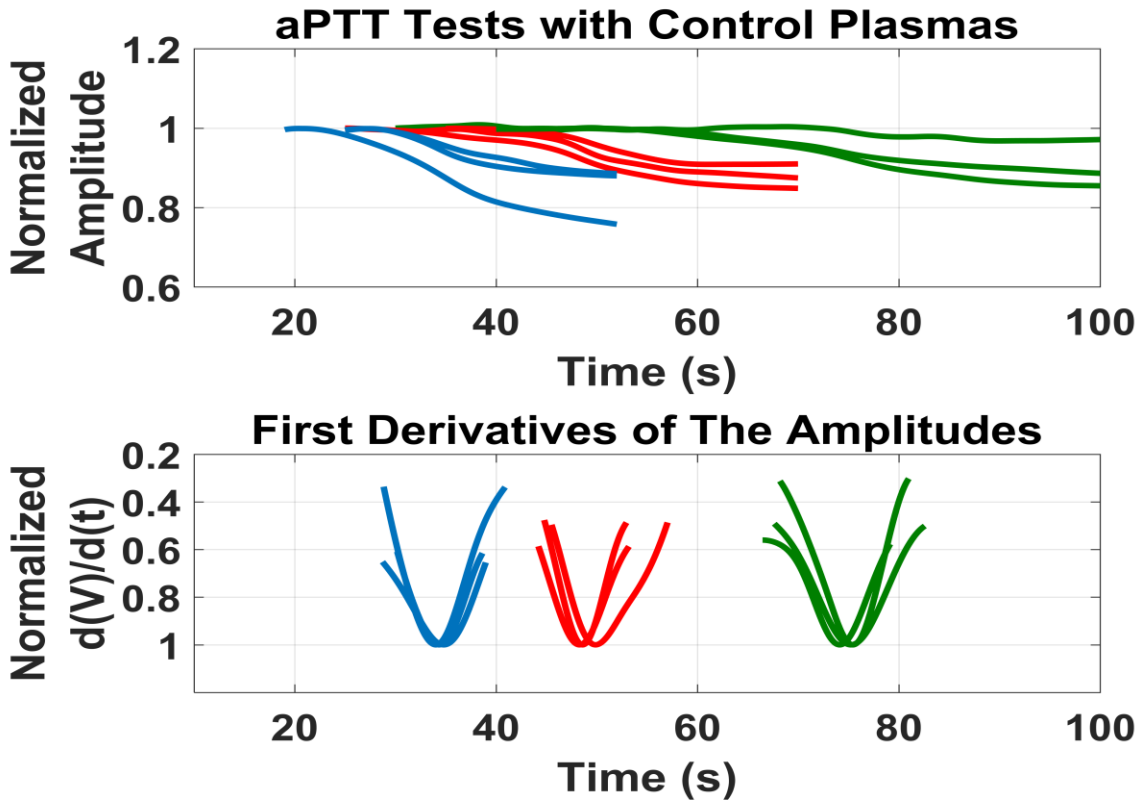

Figure 3.5 aPTT tests with normal, abnormal 1 and abnormal 2 control plasmas and first derivatives showing local minima (n=3).

	Fiber based sensor			Datasheet		
	Normalized aPTT ratio	σ	%RSD	Normalized aPTT ratio	σ	%RSD
Normal	1.03	0.014	1.36	1.03	0.007	0.68
Abnormal 1	1.45	0.007	0.48	1.4	0.015	1.05
Abnormal 2	2.22	0.012	0.54	2.2	0.038	1.73

Table 3.1 Normalized aPTT test results of control plasmas and manufacturer reference data

aPTT measurements and International Normalized Ratio (INR) for PT measurements are used for coagulation time assessments [60]. Normalized aPTT is calculated by dividing the test result by average aPTT time for the specific set-up and protocol. Average of results obtained from normal control plasma samples were equated to mean normalized aPTT value of 1.03 which is given by the manufacturer [63]. For abnormal 1 and abnormal 2 normalized aPTT values, 1.03 was used as reference. Unlike phase read out, amplitude level may change cartridge to cartridge due to light coupling condition variances and fabrication process. Therefore in addition to aPTT time normalization, amplitude levels were also normalized by dividing amplitude by the maximum amplitude value for convenient data representation. Test results well overlaps with data provided by the manufacturer [63]. There is %1.36 relative standard deviation (RSD%) for abnormal 1 and % 0.9 for abnormal tests. More comprehensive work on reproducibility of plasma coagulation tests were reported by our group [35].

3.3 aPTT tests with Whole blood

aPTT tests were conducted for demonstration of whole blood measurement capability of the proposed system. Preventing light going through blood by employing a fluid stop region enables a robust optical read out scheme as explained in section 2.2.1.

Whole blood samples were collected from a 24 years old male healthy donor. The donation of human whole blood samples from healthy donors for this study was approved by the Koç University Ethical Committee and healthy volunteers signed an informed consent. Blood samples were stored in 1.8 mL citrated blood vials (Greiner Bio One Vacuette polyethylene terephthalate sodium citrate blood collection coagulation tube, 3.2% sodium citrate). For aPTT tests, 50µL of whole blood was mixed with 50µL Micronised Silica/Platelet Substitute mixture (DIAGEN, UK, lot no: SP66). Citrated vials bind the Ca^{+} ions present in the whole blood samples. It is important to add Ca^{+} ions since Ca^{+} ions aid the fibrin formation. Since whole blood samples are citrated, coagulation process does not start until the introduction of $CaCl_2$. Therefore, mixing of $CaCl_2$ solution into mixture is taken as t = 0. While coagulation was observed through amplitude change, remaining sample was pipetted regularly and observed for clot forming as a mean of control.

3.2.1 Test protocol

- **STEP 1:** Set the temperature of the setup to 37^{o}C and wait 30 minutes to settle
- **STEP 2:** Heat a water bath to 40^{o}C
- **STEP 3:** Put 500 µL of the blood sample from citrated vials into Eppendorf tubes.

- **STEP 4:** Place the blood samples, Micronised Silica/Platelet Substitute

Mixture reagent and 25 mM CaCl2 in the heated water bath and wait at least 5 minutes

- **STEP 5:** Place cartridge onto holder. Wait 5 minutes to ensure cartridge is at 37 oC.
- **STEP 6:** Adjust in coupling and out coupling fibers for maximum DC signal using translation stages.
- **STEP 7:** Adjust PD gain and pre-amp gain accordingly. Do a wide enough frequency sweep before injecting any liquid into microchannel.
- **STEP 8:** Mix the 50 μL of reagent and the 50 μL of blood sample in an 500 μL

Eppendorf tube and wait for 5 minutes for incubation. Ensure the perfect mixing by occasional tilting.

- **STEP 9:** Mix the blood/Micronised Silica/Platelet Substitute

Mixture reagent solution with 50 μl of the 25 mM $CaCl_2$. Ensure the perfect mixing with gently pipetting 3 times. Immediately start the clock (t=0)

- **STEP 10:** Immediately place the 50 μL of the mixture into cartridge
- **STEP 11:** Do a very fast crude frequency sweep and find approximate resonance frequency. (Drive coil at that frequency and start recording amplitude and phase difference between the coil input and sensor output. Note the time on the stop watch. (The frequency doesn't need to be the exact peak resonance frequency)

STEP 12: Check the remaining mixture in the Eppendorf tube by gently pipetting for fibrin formation. Note the time on the stop watch when pipet is clogged or fibrin formation is observed.

- **STEP 13:** Monitor the sharp phase and amplitude change and record data for 180 more seconds after stabilization.
- **STEP 14:** Do a wide enough frequency sweep exactly 180 seconds after coagulation

- **STEP 15:** Remove the used cartridge from the cartridge and throw it to the medical waste bin.
- **STEP 16:** Repeat STEP 4-15 until all cartridges are tested.
- **STEP 17:** Turn off all the equipment and throw all non-usable biologic samples to medical waste bin.
- **STEP 18:** Save amplitude and phase data. Extract the first part of the data where sample insertion occurs for better assessment of the coagulation.
- **STEP 19:** Observe the amplitude drop where coagulation happens. Fit a polynomial curve to amplitude data around this drop and take first derivative of the polynomial fit. Local minimum of the signal is coagulation time.

3.2.2 Results

Measurement of whole blood was repeated 3 times from the same blood sample in order to check the reproducibility of the system. Figure 3.6 shows aPTT measurements of the blood samples taken from the same donor. Similar to control plasma tests, sharp decrease in amplitude is observed when coagulation occurs. For three different tests, coagulation times were 36, 37 and 37.5 seconds. There is no control whole blood sample readily available for coagula meter calibration since most of the laboratory coagulation tests are conducted with plasma samples. Unlike phase read out, amplitude level may change cartridge to cartridge due to light coupling condition variances and fabrication process. Therefore, amplitude levels were normalized by dividing the amplitude by maximum amplitude value for convenient data representation.

Test results of whole blood samples yielded 0.76 seconds standard deviation and %2 relative standard deviation (RSD%) encouraging a Point of Care coagula meter application for proposed system.

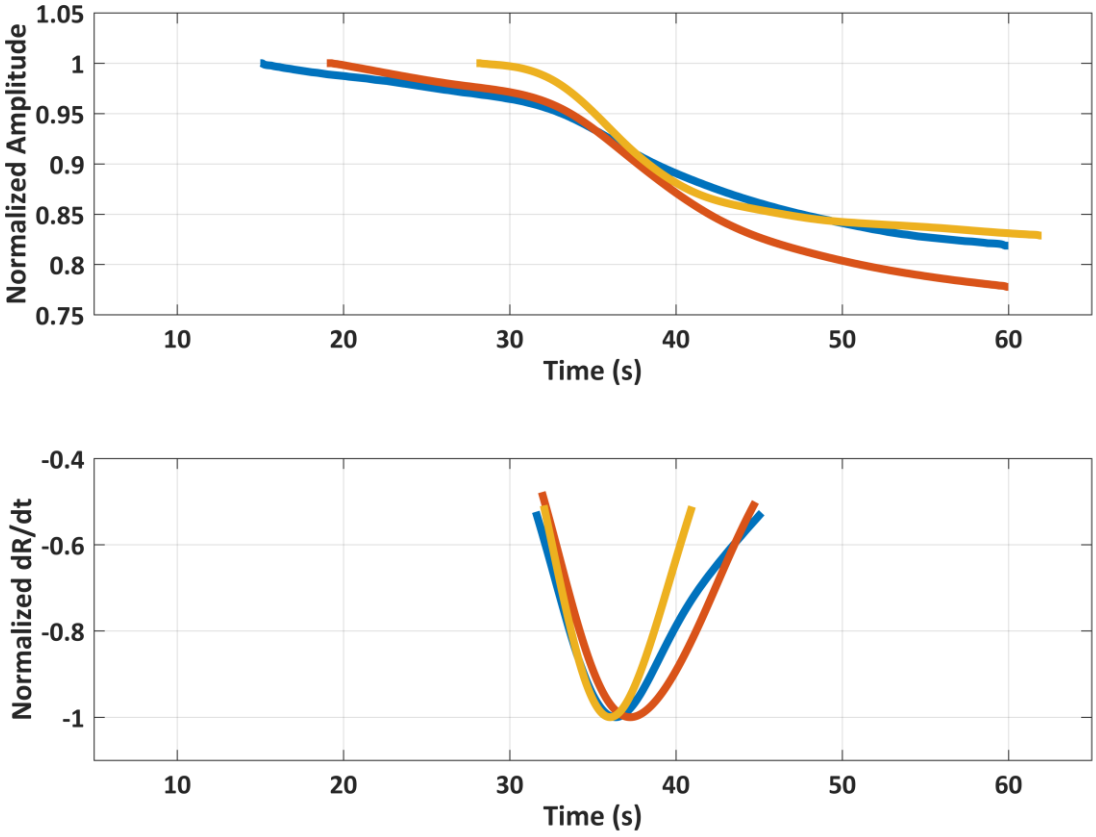

Figure 3.6 aPTT tests with whole blood samples, first derivatives showing local minima (n=3).

4 CONCLUSIONS AND FUTURE WORK

4.1 Conclusion

This thesis reports a novel optical fiber based sensor platform for coagulation time measurements from whole blood samples. This is the first report of a direct mechanical coagulation time measurement system designed for whole blood operation for point of care applications.

Developed system employs a novel optical sensor consists of two optical fibers with a small gap in between their tips mounted inside the disposable cartridge. One of the fibers acts as one-end fixed cantilever with a moving tip vibrated remotely by an electro-coil whereas the other fiber is fixed. Thus an AC optical signal is mechanically induced to light coupled to the fixed fiber. Vibrated fiber cantilever is partially submersed in blood. Any change in viscoelastic properties of the blood is monitored through modulated optical signal. Coagulation was monitored by amplitude change since amplitude of the optical signal has high SNR value exceeding 500. System was first characterized in different mediums; air, water, uncoagulated and coagulated plasma. The aPTT tests were conducted with control plasmas. Control plasma tests yielded <1% mean error and <1.36% relative standard deviation. Subsequently, whole blood aPTT capability was demonstrated using the sensor platform. Each test was repeated 3 times in order to demonstrate reproducibility of the measurements using proposed system. Test results of whole blood samples yielded 0.76 seconds standard deviation and %2 relative standard deviation (RSD%) encouraging a Point of Care coagula meter application for proposed system

One of the contributions of this work is use of a fluid stop region in order to prevent fluid leakage in between fibers. Fluid stop region utilizes capillary action; therefore, there is no physical barrier. High SNR optical read is obtained even in complex fluids such as whole blood thanks to the fluid stop region.

Another aspect of this work was developing the platform for PoC market. Thus, tolerance and fabrication issues encountered by MEMS cantilever based system previously developed in our group were overcome. In-coupling and out-coupling to the large core fibers in the cartridge proved relatively simple and has large mechanical tolerances. Current tolerance of the system is 200 μm which is ten times better than MEMS based system.

During this thesis research, a portable prototype was developed in collaboration with SFO Technologies, India. The reader unit optics, mechanics, and electronics were subsequently modified in our laboratory and became fully operational. A patent application has been filed for the proposed system and two journal articles have been drafted.

4.2 Future Work

Only aPTT tests were conducted with the proposed system. Current protocol consists of mixing of samples outside and introduction of the mixture into cartridge after coagulation cascade is initiated. Therefore, there is approximately 20 seconds of time loss. aPTT tests lasts between 35-40 seconds which is still detectable even with a 20 seconds loss but PT coagulation lasts only around 15 seconds which cannot be measured

with current protocol. Microfluidics need to be functionalized with the appropriate reagents for further implementation. Channel functionalization also enables direct coagulation measurement from freshly extracted blood. Appropriate mixing of the reagents with blood sample can be achieved by only reaction chamber functionalization. For further implementation, a simple optical sensor is needed for determining of starting time of the coagulation cascade.

As a diagnostic sensor platform, control tests and clinic tests must be conducted in large numbers for better statistics. Cartridge fabrication must be at least partly automated in order to decrease cartridge variability.

On the prototype side, some performance improvements are needed on the software part for better data acquisition. In parallel, a new prototype can be developed with more refined, user friendly and compact design.

APPENDIX A: Coagulation Curve Interpretation

Coagulation signal acquired by any continuous monitoring system has a similar trend: stable pre coagulation period, fast signal increase or decrease and stable post coagulation period. Figure A.1 shows a generic clot signal with important points on the curve [61].

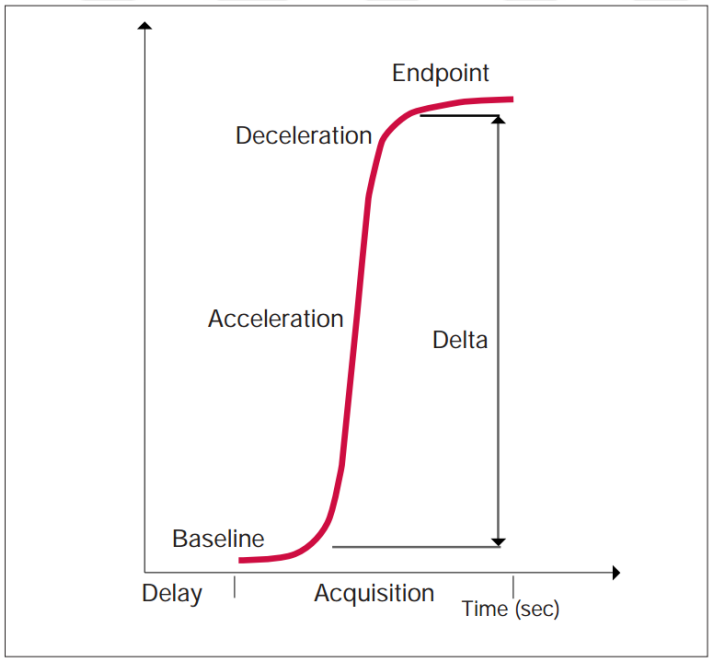

Figure A.1 Clot signal with important points [61]

It is hard to determine the exact timing of the important points from raw data. First and second derivatives of the clot curve are taken (Figure A.2). A,B,C and D denote baseline, acceleration, deceleration of clot formation and endpoint accordingly while E

denoting end of measurement. Curve is divided three main parts: pre-coagulation (A to B), Coagulation (B to D) and post –coagulation (D to E). Acceleration and deceleration of fibrin formation can be interpreted by local minimum and local maximum of second derivative respectively. Lastly, maximal rate of fibrin polymerization can be deduced by local minimum of the first derivative.

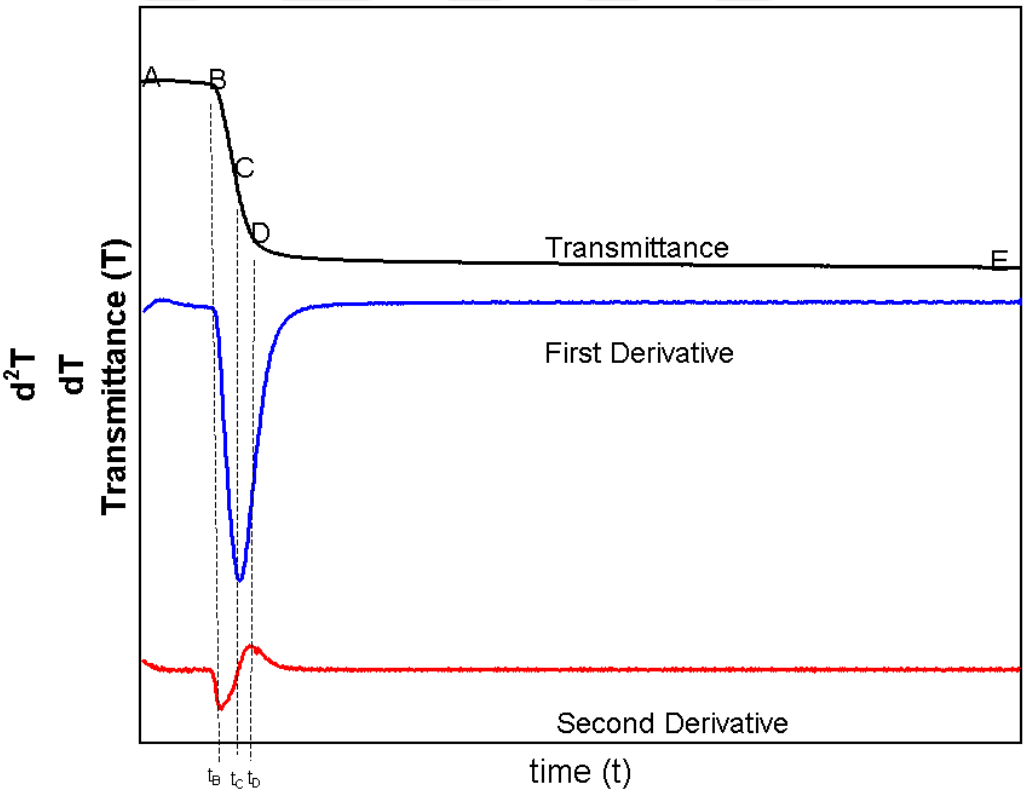

Figure A.2 First and second derivatives of the clot curve

BIBLIOGRAPHY

[1] R. F. Louie, Z. Tang, D. G. Shelby, and G. J. Kost, “Point-of-Care Testing: Millennium Technology for Critical Care,” *Lab Med.*, vol. 31, no. 7, pp. 402–408, 2000.

[2] W. Boonlert, P. H. Lolekha, G. J. Kost, and S. Lolekha, “Comparison of the Performance of Point-of-Care and Device Analyzers to Hospital Laboratory Instruments,” *Point Care J. Near-Patient Test. Technol.*, vol. 2, no. 3, pp. 172–178, 2003.

[3] A. Tejasvi, “Point-of-care diagnostics is revolutionary,” 2012. [Online]. Available: http://www.biospectrumasia.com/biospectrum/analysis/123299/point-care-diagnostics-revolutionary.

[4] D. C. Klonoff, “Point-of-care blood glucose meter accuracy in the hospital setting,” *Diabetes Spectr.*, vol. 27, no. 3, pp. 174–179, 2014.

[5] A. Jain, I. Subhan, and M. Joshi, “Comparison of the point-of-care blood gas analyzer versus the laboratory auto-analyzer for the measurement of electrolytes,” *Int. J. Emerg. Med.*, vol. 2, no. 2, pp. 117–120, 2009.

[6] L. F. Harris, V. Castro-López, and A. J. Killard, “Coagulation monitoring devices: Past, present, and future at the point of care,” *TrAC - Trends Anal. Chem.*, vol. 50, pp. 85–95, 2013.

[7] K. W. Davie E.W., Fujikawa K., “The Coagulation Cascade: Initiation, Maintenance, and Regulation,” *Biochemistry*, vol. 30, no. 43, 1991.

[8] B. B. C. Furie and B. B. C. Furie, “Review series Thrombus formation in vivo,” *J. Clincial Investig.*, vol. 115, no. 12, pp. 3355–3362, 2005.

[9] W. Korte, K. Gabi, M. Rohner, A. Gahler, C. Szadkowski, T. W. Schnider, J. Lange, and W. Riesen, “Preoperative fibrin monomer measurement allows risk stratification for high intraoperative blood loss in elective surgery.,” *Thromb. Haemost.*, vol. 94, no. 1, pp. 211–215, Jul. 2005.

[10] V. L. Ng, “Liver Disease, Coagulation Testing, and Hemostasis,” *Clin. Lab. Med.*, vol. 29, no. 2, pp. 265–282, Jun. 2009.

[11] S.-W. Lin, Y.-C. Chuang, Y.-S. Lin, H.-Y. Lei, H.-S. Liu, and T.-M. Yeh, “Dengue virus nonstructural protein NS1 binds to prothrombin/thrombin and inhibits prothrombin activation.,” *J. Infect.*, vol. 64, no. 3, pp. 325–334, Mar. 2012.

[12] S. Lison and M. Spannagl, “Monitoring of direct anticoagulants,” *Wiener Medizinische Wochenschrift*, vol. 161, no. 3–4, pp. 58–62, 2011.

[13] J. W. Ojito, R. L. Hannan, M. M. Burgos, H. Lim, M. Huynh, E. Velis, M. Arocha, C. F. Tirotta, and R. P. Burke, “Comparison of point-of-care activated clotting time systems utilized in a single pediatric institution.,” *J. Extra. Corpor. Technol.*, vol. 44, no. 1, pp. 15–20, 2012.

[14] C. M. Jackson and M. P. Esnouf, “Has the time arrived to replace the quick prothrombin time test for monitoring oral anticoagulant therapy?,” *Clin. Chem.*, vol. 51, no. 3, pp. 483–485, 2005.

[15] M. T. Ganter and C. K. Hofer, “Coagulation monitoring: current techniques and clinical use of viscoelastic point-of-care coagulation devices.,” *Anesth. Analg.*, vol. 106, no. 5, pp. 1366–1375, May 2008.

[16] C. P. M. Hayward, K. A. Moffat, E. Plumhoff, and E. M. Van Cott, “Approaches to investigating common bleeding disorders: an evaluation of North American coagulation laboratory practices.,” *Am. J. Hematol.*, vol. 87 Suppl 1, pp. S45–50, May 2012.

[17] G. C. White, “The partial thromboplastin time: Defining an era in coagulation,” *J. Thromb. Haemost.*, vol. 1, no. 11, pp. 2267–2270, 2003.

[18] J. Hirsh, L. Poller, D. Deykin, M. Levine, and J. E. Dalen, “Optimal therapeutic range for oral anticoagulants,” *Chest*, vol. 95, no. 2 SUPPL., pp. 5–11, 1989.

[19] R. A. Marlar, D. Ph, P. J. Bauer, M. T. Ascp, J. L. Endres-brooks, and M. T. Ascp, “Comparison of the Sensitivity of Commerciai APTT Reagents in the Detection of Mild Coagulopathies,” pp. 436–439, 1984.

[20] M. H. Qari, “High throughput coagulation analyzers review.,” *Comb. Chem. High Throughput Screen.*, vol. 8, no. 4, pp. 353–360, Jun. 2005.

[21] M. Heins and H. Reinauer, “Automation in coagulation testing.,” *J. Int. Fed. Clin. Chem.*, vol. 8, no. 3, pp. 117–122, 1996.

[22] J. A. Koepke, “Technologies for coagulation instruments,” *Lab. Med.*, vol. 31, no. 4, pp. 211–215, 2000.

[23] S. Kitchen and M. Makris, “Laboratory Tests of Hemostasis,” in *Practical Hemostasis and Thrombosis*, Blackwell Publishing Ltd, 2007, pp. 8–17.

[24] D. Pacaud, J.-F. Lemay, P. Guay, M. Buithieu, and J.-F. Yale, “ASSESSMENT OF BLOOD VOLUMES OBTAINED BY CAPILLARY PUNCTURES IN OLDER CHILDREN AND ADOLESCENTS WITH DIABETES. [dagger] 558,” *Pediatr Res*, vol. 39, no. S4, p. 95, Apr. 1996.

[25] C. C. Shih, C. M. Shih, Y. Y. Su, L. H. J. Su, M. S. Chang, and S. J. Lin, “Quantitative evaluation of thrombosis by electrochemical methodology,” *Thromb. Res.*, vol. 111, no. 1–2, pp. 103–109, 2003.

[26] D. Barcellona, L. Fenu, S. Cornacchini, and F. Marongiu, “Point-of-care (POCT) prothrombin time monitors: is a periodical control of their performance useful?,” *Thromb. Res.*, vol. 123, no. 5, pp. 775–779, Mar. 2009.

[27] A. R. Corno, R. Redaelli, T. M. Caimi, L. Borroni, G. M. Somaini, G. Mostarda, E. Morra, and G. Gesu, “THE NEW microINR POINT OF - CARE SYSTEM IN ORAL ANTICOAGULANT THERAPY MONITORING,” vol. 5, p. 5.

[28] R. S. Lakshmanan, V. Efremov, S. M. Cullen, and A. J. Killard, “Measurement of the evolution of rigid and viscoelastic mass contributions from fibrin network formation during plasma coagulation using quartz crystal microbalance,” *Sensors Actuators, B Chem.*, vol. 192, pp. 23–28, 2014.

[29] M. Hussain, “Ultra-sensitive detection of heparin via aPTT using plastic antibodies on QCM-D platform,” *RSC Adv.*, vol. 5, no. 68, p. 54963, 2015.

[30] M. M. Tripathi, Z. Hajjarian, E. M. Van Cott, and S. K. Nadkarni, “Assessing blood coagulation status with laser speckle rheology,” *Biomed. Opt. Express*, vol. 5, no. 3, p. 817, 2014.

[31] X. Xu, J. Zhu, and Z. Chen, “Dynamic and quantitative assessment of blood coagulation using optical coherence elastography,” *Sci. Rep.*, vol. 6, no. April, p. 24294, 2016.

[32] A. Jain, A. Graveline, A. Waterhouse, A. Vernet, R. Flaumenhaft, and D. E. Ingber, “A shear gradient-activated microfluidic device for automated monitoring of whole blood haemostasis and platelet function.,” *Nat. Commun.*, vol. 7, p. 10176, 2016.

[33] C. L. Yang, S. J. Huang, C. W. Chou, Y. C. Chiou, K. P. Lin, M. S. Tsai, and K. C. Young, “Design and evaluation of a portable optical-based biosensor for testing whole blood prothrombin time,” *Talanta*, vol. 116, pp. 704–711, 2013.

[34] S. L. Karsten, M. C. Tarhan, L. C. Kudo, D. Collard, and H. Fujita, “Point-of-care (POC) devices by means of advanced MEMS,” *Talanta*, vol. 145, pp. 55–59, 2015.

[35] O. Cakmak, E. Ermek, N. Kilinc, S. Bulut, I. Baris, I. H. Kavakli, G. G. Yaralioglu, and H. Urey, “A cartridge based sensor array platform for multiple coagulation measurements from plasma,” *Lab Chip*, vol. 15, no. 1, pp. 113–120, 2015.

[36] O. Cakmak, C. Elbuken, E. Ermek, A. Mostafazadeh, I. Baris, B. Erdem Alaca, I. H. Kavakli, and H. Urey, “Microcantilever based disposable viscosity sensor for serum and blood plasma measurements,” *Methods*, vol. 63, no. 3, pp. 225–232, 2013.

[37] O. Cakmak, E. Ermek, H. Urey, G. G. Yaralioglu, and N. Kilinc, “MEMS based blood plasma viscosity sensor without electrical connections,” *IEEE SENSORS 2013 - Proc.*, 2013.

[38] A. Mostafazadeh, G. G. Yaralioglu, and H. Urey, “Optical fiber array based simultaneous parallel monitoring of resonant cantilever sensors in liquid,” *Sensors Actuators, A Phys.*, vol. 242, pp. 132–139, 2016.

[39] C. A. Van Eysden and J. E. Sader, “Frequency response of cantilever beams immersed in viscous fluids with applications to the atomic force microscope: Arbitrary mode order,” *J. Appl. Phys.*, vol. 101, no. 4, 2007.

[40] J. E. Sader, J. W. M. Chon, and P. Mulvaney, “Calibration of rectangular atomic force microscope cantilevers,” *Rev. Sci. Instrum.*, vol. 70, no. 10, pp. 3967–3969, 1999.

[41] J. W. M. Chon, P. Mulvaney, and J. E. Sader, “Experimental validation of theoretical models for the frequency response of atomic force microscope cantilever beams immersed in fluids,” *J. Appl. Phys.*, vol. 87, no. 8, pp. 3978–3988, 2000.

[42] C. Wang, H.-H. Yu, M. Wu, and W. Fang, “Implementation of phase-locked loop control for MEMS scanning mirror using DSP,” *Sensors Actuators A Phys.*, vol. 133, no. 1, pp. 243–249, Jan. 2007.

[43] M. K. and T. M. and J. L. S.-R. and A. B. and U. Schmid, “Q -factor enhancement for self-actuated self-sensing piezoelectric MEMS resonators applying a lock-in driven feedback loop,” *J. Micromechanics Microengineering*, vol. 23, no. 8, p. 85009, 2013.

[44] J. Kalenik and R. Pajgk, “A cantilever optical-fiber accelerometer,” vol. 65, pp. 350–355, 1998.

[45] M. Lo, “Measuring Element,” 1996.

[46] J. M. S. Sakamoto, C. Kitano, G. M. Pacheco, and B. R. Tittmann, “High sensitivity fiber optic angular displacement sensor and its application for detection of ultrasound,” *Appl. Opt.*, vol. 51, no. 20, pp. 4841–4851, 2012.

[47] A. I. Fedorchenko, I. Stachiv, J. N. Ho, A. B. Wang, and W. C. Wang, “On the forced vibration of the fiber partially immersed in fluid,” *Sensors Actuators, A Phys.*, vol. 147, no. 2, pp. 498–503, 2008.

[48] A. I. Fedorchenko, I. Stachiv, and A. B. Wang, “The optical viscometer based on the vibrating fiber partially submerged in fluid,” *Sensors Actuators, B Chem.*, vol. 142, no. 1, pp. 111–117, 2009.

[49] C. Ziegler, “Cantilever-based biosensors,” *Anal. Bioanal. Chem.*, vol. 379, no. 7, pp. 946–959, 2004.

[50] C. Vančura, I. Dufour, S. M. Heinrich, F. Josse, and A. Hierlemann, “Analysis of resonating microcantilevers operating in a viscous liquid environment,” *Sensors Actuators A Phys.*, vol. 141, no. 1, pp. 43–51, Jan. 2008.

[51] A. H. Cherin and P. J. Rich, “Method of splicing pairs of arrayed or individual fibers utilizing optical fiber aligning grooves.” Google Patents, 1977.

[52] A. N. Yaroslavsky, I. V Yaroslavsky, T. Goldbach, and H.-J. Schwarzmaier, “Optical properties of blood in the near-infrared spectral range,” 1996, vol. 2678, pp. 314–324.

[53] D. J. Guckenberger, T. de Groot, A. M.-D. Wan, D. Beebe, and E. Young, “Micromilling: A method for ultra-rapid prototyping of plastic microfluidic devices,” *Lab Chip*, vol. 15, no. 11, pp. 2364–2378, 2015.

[54] Y. Cai, Z. Liu, Z. Shi, Q. Song, and Y. Wan, “Optimum end milling tool path and machining parameters for micro Laval nozzle manufacturing,” *Proc. Inst. Mech. Eng. Part B J. Eng. Manuf.*, p. 0954405415608601, 2015.

[55] K. Ren, J. Zhou, and H. Wu, “Materials for microfluidic chip fabrication,” *Acc. Chem. Res.*, vol. 46, no. 11, pp. 2396–2406, 2013.

[56] L. Xie, C. S. Premachandran, M. Chew, S. C. Chong, L. C. Wai, and J. Lau, “Optimization of a Microfluidic Cartridge for Lab-on-a-Chip (LOC) Application and Bio-Testing for DNA / RNA Extraction,” no. May, 2008.

[57] S. Z. Lulec, C. Sagiroglu, A. Mostafazadeh, E. Ermek, E. Timurdogan, Y. Leblebici, and H. Urey, “Simultaneous self-sustained actuation and parallel readout with MEMS cantilever sensor array,” *Micro Electro Mechanical Systems (MEMS), 2012 IEEE 25th International Conference on*. pp. 644–647, 2012.

[58] A. S. Wolberg, Z. H. Meng, D. M. Monroe, and M. Hoffman, “A Systematic Evaluation of the Effect of Temperature on Coagulation Enzyme Activity and Platelet Function,” *J. Trauma Inj. Infect. Crit. Care*, vol. 56, no. 6, pp. 1221–1228, 2004.

[59] L. Muller, S. Sinn, H. Drechsel, C. Ziegler, H.-P. Wendel, H. Northoff, and F. K. Gehring, “Investigation of prothrombin time in human whole-blood samples with a quartz crystal biosensor.,” *Anal. Chem.*, vol. 82, no. 2, pp. 658–663, Jan. 2010.

[60] S. Yuan, C. Ferrell, and W. L. Chandler, “Comparing the prothrombin time INR versus the APTT to evaluate the coagulopathy of acute trauma,” *Thromb. Res.*, vol. 120, no. 1, pp. 29–37, 2007.

[61] K. Doubleday and S. Kumnick, “Clot Signature Curves and the ACL Advance,” *Instrum. Lab.*, 2001.

[62] “Fiber Coupling Effiency Calculation,” *Doric LEnses*, no. 418, pp. 1–4, 2007.

[63] Coagucheck XS. (15.06.2014). *Evaluation Report 06024, Roche, Germany*. Available:

http://www.roche.co.uk/content/dam/internet/corporate/roche/en_GB/documents/Evaluation_Report_-_CoaguChek_XS.pdf

VITA

Yusuf Samet Yaraş was born in Antalya, Turkey, in 1990. He received his B.Sc. degree in Electronics Engineering (with high merit scholarship) from Sabancı University, Istanbul, Turkey, in 2013. Since then, he has been working at Optical Microsystems Laboratory (OML) of Koç University, Department of Electrical Engineering as a M.Sc. candidate. He also spent 5 months at Georgia Institute of Technology, US as a visiting researcher. He will join electrical engineering department of Georgia Institute of Technology,USA to pursue his PhD degree.

Yusuf Samet Yaraş is the co-inventor of 2 pending PCT patents.